Politecnico di Torino

DIPARTIMENTO DI INGEGNERIA MECCANICA E AEROSPAZIALE
Corso di Laurea Magistrale in Ingegneria Aerospaziale

Progetto preliminare di un long-range, twin-engine turboprop per missioni di tipo SaR e Maritime Patrol.

Candidato:
GM (CP) Flavio Marangi
Matricola 221885

Relatore:
Prof. Giulio Romeo

Correlatore:
Prof. Enrico Cestino

Anno Accademico 2018-2019

Progetto preliminare di un long-range, twin-engine turboprop per missioni di tipo SaR e Maritime Patrol.

Flavio Marangi
Politecnico di Torino

7 ottobre 2019

A Michele Marangi
“Possa tu un giorno sentirti realizzato per le mie azioni
come tuo padre lo è stato per le tue”

Indice

Elenco delle figure

Elenco delle tabelle

Introduzione

Con l'attuazione della legge n. 979 del 31 dicembre 1982 recante "Disposizioni per la difesa del mare" nasce la Componente Aerea della Guardia Costiera. In particolare essa si inquadra nel più ampio impegno di istituzione di un "servizio di vigilanza e soccorso" mediante l'acquisizione di aeromobili da parte della Guardia Costiera. La stessa, istituita con Decreto Interministeriale dell'8 giugno 1989, segue la nuova articolazione delle Capitanerie di Porto ed è costituita dall'inglobamento dei reparti aeronavali preesistenti.
Fondamentali le funzioni svolte dalla componente aerea quali la ricerca di naufraghi e di unità navali ed aeree in difficoltà in mare, il soccorso a naufraghi ed a traumatizzati ed ammalati a bordo di navi (tramite recupero con il verricello e/o aviolancio di battelloni), la tutela dell'ambiente marino e delle aree marine protette anche a mezzo di sistemi di telerilevamento sia per monitoraggio periodico e sistematico che in occasione di eco-emergenze. Importante anche le attività di vigilanza sulla pesca marittima e sull'acquicoltura finalizzate al rispetto delle normative nazionali e comunitarie nonché sulla navigazione e sulle attività marittime che si svolgono nelle acque territoriali e di interesse nazionale, con particolare riferimento alla sicurezza della navigazione e alla salvaguardia della vita umana in mare nella sua accezione più ampia.

A tale scopo, questo lavoro vuole essere una valida proposta di un nuovo velivolo multi-missione che si configuri come evoluzione dei modelli esistenti e ad oggi presenti sul mercato.
È importante notare come il design di un aereo segua un andamento altalenante costellato di compromessi e limiti dei quali è fondamentale riconoscerne e quindi capirne l'influenza sulle varie configurazioni del velivolo.
Il lavoro qui presentato si inquadra nella fase di sviluppo di un velivolo denominata *"Project Design"*. In particolare, essendo questa composta da tre fasi che si susseguono più o meno linearmente lungo la linea temporale di evoluzione del progetto, questa tesi si pone nella posizione iniziale di detta linea andando a rappresentare l'oggetto delle fasi di *"Conceptual Design"* e *"Preliminary Design"*.
Dette fasi hanno come "regole di ingaggio" lo sviluppo di un certo numero di soluzioni che rispettino i requisiti richiesti al velivolo da implementare. In particolare questo lavoro vuole proporre una di queste soluzioni la quale, al fine di adempiere a tutti i doveri imposti dal *Convivio*, verrà descritta seguendo passo passo tutte le analisi che la caratterizzano.

Ringraziamenti

Durante la stesura di questa tesi, un grande numero di persone mi hanno assistito dandomi informazioni, supporto ed incoraggiamento.

Sicuramente un doveroso ringraziamento è dovuto al Prof. Ing. Giulio Romeo e al Prof. Enrico Cestino che costantemente mi hanno supportato nello sviluppo del progetto fin dal suo concepimento.

È per me fondamentale ringraziare i miei parenti ed in particolare i miei genitori che sempre, anche nei momenti più bui, mi hanno dato la forza e la motivazione per arrivare al traguardo di questa parte della mia vita.

Importante è riconoscere il supporto ricevuto dagli uffici dell'Organo Centrale di Sicurezza del Ministero delle Infrastrutture e dei Trasporti, ed in particolare dal Dirigente Generale Dott. Costantino Fiorillo e dal CV (AN) Dario Sgobbi, i cui insegnamenti sono per me fonte di quotidiana ispirazione.

Va inoltre ricordato l'aiuto dei miei amici che sempre si sono interessati al mio lavoro, fornendomi spunti di riflessione e informazioni utili allo svolgimenti dei vari approfondimenti.

In ultimo un ringraziamento speciale vuole essere riservato alla mia più cara amica Valentina, per la generosità e la dedizione che ogni giorno mette in atto affinché io non perda mai di vista i miei obiettivi.

Capitolo 1

Market Outlook

New aircraft design requires a huge amounts of efforts in terms of time, people and budget. For this reason manufacturers approach new aircraft design just when they foresee to cover a specific market sector with low risk and high profit margin. Consequently, every year detailed analyses are carried out from aircraft manufacturers as to investigate aircraft industry relating to oil market and global and region economy.
Most important factor for future aircraft industry are:

- Economic growth
- Oil price and volatility
- Emerging markets
- Scope clause relaxation
- More efficient aircraft
- Environmental regulation and fees

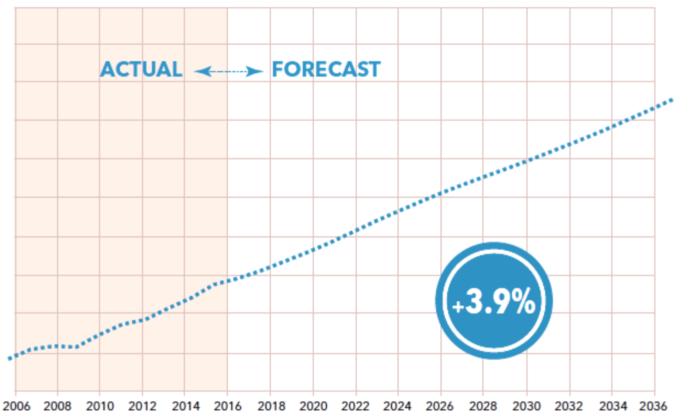

Figura 1.1: Actual and expected average annual traffic growth [2]

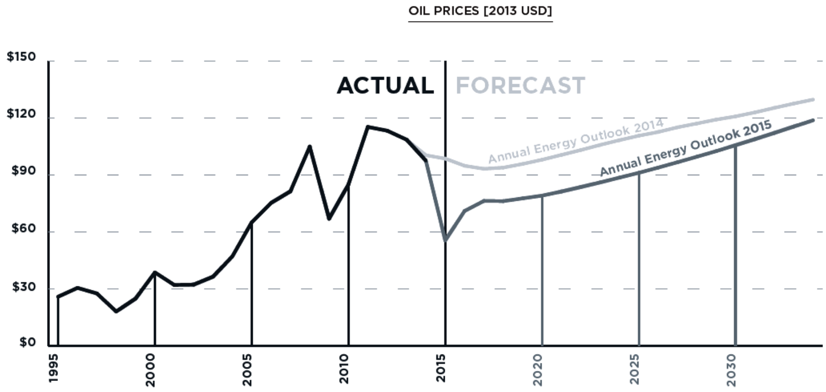

Figura 1.2: Actual oil prices and comparison in forecast oil price between 2014 and 2015 [3]

In 2017 the world economy is forecasted to grow 3.0% driven by improvements in advanced economies and by lower commodity prices in emerging markets. Although economic instability resulting from geopolitical factors in the Commonwealth of Independent States (CIS), Middle East and North Africa, the global growth should pick up considerably in 2018 achieving an average annual traffic growth of 3.9% [2] [4].
Next to this positive data, aircraft manufactures have to deal with the volatile fuel prices that are forecasted to increase in the long-term. For airline company this means increasingly high operating cost with need of more efficient fleet.
Oil production in the future will be hardest, slower to extract and with more polluting. Therefore to reach positive financial results it is essential to answer market requests with optimal solutions capable to enhance economy in emerging market and to determine a strong environmental appeal in the mature market.

In consequence to the traffic growth, adding more seats and consequently adding bigger airplanes is not necessarily the best solution. Aircraft industry is notoriously cyclical. For example in economic downturn, when demand drops and consumers reduce expenses, the effect of overcapacity is reflected in both trip cost and weaker yields. A more prudent and smart solution to increasing capacity and flight frequency while preserving unit revenues is provided by aircraft in the 70 to 130-seat segment. As a manufacturer, our aim is to offer products that ensure offer value and sustainable revenues for our customers as they navigate an ever-changing marketplace. Having 70 to 130- seat aircraft with their flexibility to add capacity with minimal risk is good for the bottom line and, equally important, when measuring asset performance.

Confirmation of this particular seat segment aircrafts is in the regional aviation market that has evolved rapidly over recent years, both from a geographical and technological point of view and from a business model perspective. It is not just about linking with more frequency megacities of the world, but also about revealing the potential of secondary and tertiary airports. Thanks to a combination of reduction in fuel burn, increasingly velocity and noise reduction,

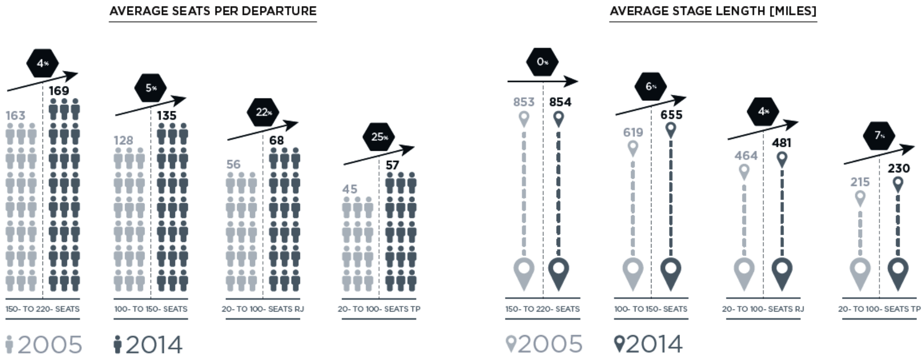

Figura 1.3: Comparison in average seats per departure and average stage length amount different airplane seat-segments from 2005 and 2014 [3].

turboprops have a key role to play in exploring and developing new routes, thus promoting local community development and being a friendly option for city centres as well.

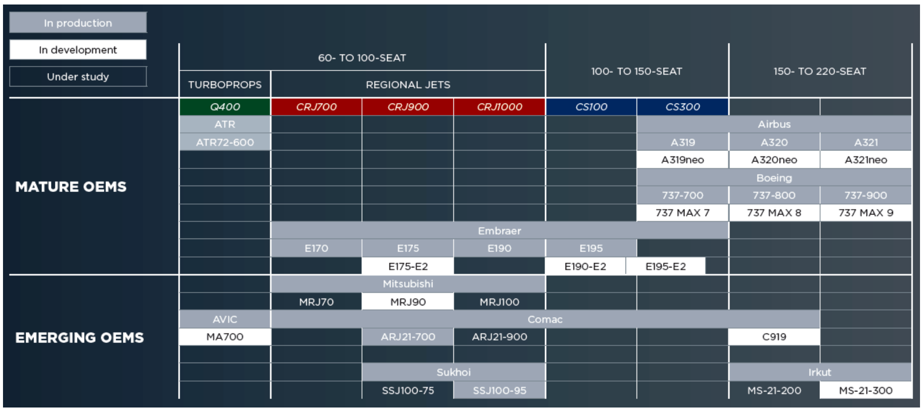

Figura 1.4: Overview of aircraft models competitor in 60- to 220- seat segment. Aircraft are banded together in production, development and under study [3].

Commercial airlines are profitable and growing; and the industry continues to evolve to manage growth, volatile fuel prices and increasing competition. Through a competitive landscape in three different seat segments there is an obvious room to growth for turboprops with their more attractive features respect to turbojets right in the segment where is expected the highest delivery request. Opportunities are available both in mature and emerging markets.

Most new 60- to 150- seat aircraft deliveries to mature aviation markets will replace retiring aircraft fleets. While in emerging markets, demand for air travel is growing with increasing GDP and an expanding middle class. As is possible to see from 1.5, the GDP per capita growth is related to substantial improves in prospective for regional aviation, especially when country adopt regional air connectivity to accelerate economic growth.

Although lower oil prices may permit airline carriers to delay the replacement or retirement of less efficient aircraft types, in the long-term, fuel efficiency and adaptability will be keys driver of airline fleet decisions. Economic and technological obsolescence, as well as environmental regulations, are expected to drive aircraft retirements throughout the forecast. In consequence of data showed earlier in 1.3 and 1.5 is confirmed an increase of turboprops utilization over regional jet. From 2006 to 2016 regardless of the fuel price, turboprops extended their operational scope, and in the long-term prospect turboprops are going to be the preferred choice for short commercial hauls.

Analyzing deeper statistics about average traffic growth is possible to recognize interesting information on growth contribution. In 1.6 is showed how in 2006, 2015 and 2035 is divided turboprop market growth. In each analyzed year is clear the important percentage of existing network growth and new route creation respect to upsizing to larger capacity. Specifically from 2006 to 2035 the percentage of existing network growth and new route creation increase continuously over upsizing percentage. For instance, in 2035 for ATR the the half of this growth is driven by the creation of new routes as part of airlines network development strategy.

Equally important is to examine the forecast on turboprop fleet evolution and deliveries. In this case ATR and Embraer agree with a prevision on 86% more of turboprop deliveries in the next 20 years.

1.1 Regional market review

In this section, as stated above, it is being used studies performed by ATR in 2015 [2] and Embraer[4] for the specific turboprop's market investigation.
The turboprop market is flourishing towards China (from 1% to 9%) and South America (from 10% to 13%) as it is schematized in 1.7.

The fleet in service in each country will increase in the period 2015-2035, but not in the same way (see 1.8). China will rise from 35 turboprop in service in 2015 to 320 in 2035 (it means an annual growth rate of 40.7%) followed by South America which rises from 220 turboprops to 500. In the last position of the ranking appears North America, with 450 turboprops in 2015 and will achieve 650 aircrafts powered by propeller in 2035 with an annual growth rate of 2.2%.

Before getting to the substance it is sum up in 1.9 the economical investments in air transport according to the area. The graphic it has been built from data extracted from [5].

In addition there are differences in the demands of each country depending on the type of economy. As it can be seen in 1.10, emerging markets' demand has overtaken the mature markets' capacity since 2011 in the regional sector.

The demand in emerging countries is expected to grow eight times faster than that of mature economies. Moreover the quality of regional network is essential to balance economic growth, and as it is showed in 1.11, there is a strong potential for the most populated countries (China and India) to enhance their regional network and link the most remote communities.

In next sections it will be discussed each region by order of importance to analyzed it deeply ([5]) :

- Northeast Asia
- Southeast Asia
- China
- Oceania
- Northern America
- Southern America
- Europe
- Africa

1.1.1 Northeast Asia

As is possible to see from the graph in Figure 1.12, the Asian region will suffer an increase from the 29% of the revenue passenger kilometres (RPK) until 36% in 2034, taking into account the rises in the internal market, so many companies will be able to offer new services with new or modified characteristics [6].

Northeast Asia, which includes Japan, North and South Korea and Taiwan, accounts for 10 percent of world gross domestic product (GDP). Although the region's GDP is growing more slowly than the world average, it is expected to maintain a sustaining rate of 1.3 percent over the next 20 years. This growth will result in a need for 1,450 new airplanes. Also northeast Asia is interesting because two-thirds of new airplanes will replace existing airplanes, and the remaining one-third will respond to airline growth in the region.

It should be underlined that the high rise in tourism will cause the modernization of infrastructures and at the same time will require the creation of new ones to supply the demand. Additionally, it has to be given a particular emphasis to the Japanese economy that among Fukushima's disaster (11th of March 2011) it is still leading the list of dominant economies. The main potential of northeast Asia is the increase in demography, that creates a big rise in the services to fulfil the demands, developing a boost in exportations and importations.

1.1.2 Southeast Asia

Economic growth in Southeast Asia has averaged more than 5 percent annually for the past decade and is forecast to continue expanding at the slightly lower rate of 4.6 percent through 2034. Nine of the top 10 major industries in the region are of the type that tends to drive air travel. As it could be seen in the graph1.13, where the turboprop aircrafts are included in Single Aisle airplanes, they will increase from 900 (2014) to 3150 units (2034), creating a bigger proportion of Single Aisle airplanes in the share of fleet.

1.1.3 China

This nation, influenced for the population (1.4 MM in 2013) and for its economy, is in the middle of the golden age in a moment of world crisis. China will increments the GDP from 6.4% to 8.5% the following 20 years. It is also expected that in the following years it will reach a 16% of the world GDP. The internal aerial transport it has raised 10.6% compared to the precedent years and it will raise 20% the following ones. New airports and other infrastructure will be needed to satisfied the growth.

As it could be seen in the graph1.14, where the turboprop aircrafts are included in Single Aisle airplanes, the proportion of this kind of airplanes will increase from 2060 (2014) to 5340 units (2034), creating a bigger proportion of Single Aisle airplanes in the share of fleet.

1.1.4 Oceania

Oceania is a really dynamic region for the modestly low density of population, there is not so many people in a big area (like in Australia), and it creates a huge demand in air transport to be able to create internal links. The annual growth is 4.8% for the internal and external travels for the next 20 years. Furthermore there will be an increasing of 5% for the travels from Oceania to South Asia. The airlines in this continent are growing as a response to the worldwide competition, specially Eastern Asia, to supply all the demands. It is expected that they will need 1010 new airplanes to be able to satisfy transport requirements. Focusing in turboprops' market, in the graph1.15, the proportion of this kind of airplanes (Single Aisle) will increase from 400 (2014) to 750 units (2034), creating a bigger proportion of Single Aisle airplanes (77%) in the share of fleet.

1.1.5 North America

The American industry is developing in an stable economy, caused by the fusion and links between aeronautical companies and airlines, creating new enterprises that controls up to 85% of the American's air transport market. Air traffic in North America will grow with an annual rate of 2.7%, and studying in detail the turboprop's market, in the graph 1.16, the proportion of turboprops (included in Single Aisle airplanes) will increase from 3850 (2014) to 6190 units (2034), creating a bigger proportion of Single Aisle airplanes (64%) in the share of fleet.

1.1.6 South America

Economic growth in Central America remains strong, led by Panama with growth averaging 5.6% over the next five years. Meanwhile, five-year average growth rates for Brazil and Mexico are 3.8% and 2.3%, respectively. Aviation is a key component of this growth dynamic because it facilitates trade, travel, and tourism, while promoting globalization and technology development. It will be an strong demand for air travel over the long term for South America.

Focusing in turboprops' market, in the graph1.17, the proportion of turboprop airplanes will increase from 1220 (2014) to 3020 units (2034), creating a bigger proportion of Single Aisle airplanes (84%) in the share of fleet.

1.1.7 Europe

The European market remained strong until the beginning of the economical crisis, after that, the future is uncertain but current studies reveal that the European GDP will rise 1.8% each year until 2032. Recently the European airlines have added 1.5% passengers and they own 230 new aircrafts than two years before. In the next 20 years the European aerial companies will acquire 7560 new airplanes with a total cost of 11000 $ billion. Looking at turboprops' market, in the graph1.18, the proportion of this kind of airplanes (Single Aisle) will increase from 3240 (2014) to 5730 units (2034), creating a bigger proportion of Single Aisle airplanes (79%) in the share of fleet.

The tendency in the aerial operators is focused in develop new short and long range routes with the low-cost's characteristics. To make it possible next years will be performed acquisitions of small airlines by big companies, and with these fusions a better collaboration worldwide will be possible.

1.1.8 Africa

The African continent has quite good economical prospectives for the following years, but due to the unstable politics and the low number of aerial infrastructures the growth is not as huge as in other regions. In one hand the tourism is varying depending on the problems between (and also inside) each country, then it is not possible to do a trustable forecast. On the other hand, urbanization and economic growth are intricately related as agrarian-based regional economies transition to urban economies centred on industry and services. Successful conversion requires a shift in spending to projects that focus on integrated urban planning to improve infrastructure, spur productivity, and foster income growth. The increase in urbanization and economic growth, meanwhile, is expected to stimulate demand for air travel to, from, and within the continent.

As it could be seen in the graph1.19, where the turboprop aircrafts are included in Single Aisle airplanes, they will increase from 430 (2014) to 1220 units (2034), creating a bigger proportion (71%) of Single Aisle airplanes in the share of fleet.

In order to conclude the part of the chapter regarding civil application, it is attached a graphic summary of the main important data in Figure 1.20:

1.2 Military Market Aircraft

Despite massive cuts in defence procurement and significant austerity measures, North-America, Europe and notably Asia, are expected to account for a significant portion of the total military aircraft, with shares of 42.9% , 24.1% and 21.8% .

Figura 1.21: The global military aircraft market by region - 2011-2021 [7]

Investment in Intelligence, reconnaissance and surveillance (ISR) is growing, driven by countries involved in border disputes with neighbours, as well as those investing in maintaining high alertness and deterrence.

Multi-role aircraft category is expected to account for the highest proportion of spending in the global military aircraft market due to its suitability to perform multiple missions, therefore better adapting to offer savings mandated by budget cuts. Multi-mission aircraft are commonly applied to various missions including reconnaissance, rescue operations and transport.

To increase the capabilities of modern military aircraft, the global defence industry is investing significantly in R&D which has led to the development of technologies to enhance the speed, power, stealth capabilities, destructive force and take-off and landing capabilities of the various types of military aircraft.

1.2.1 Case Example: EADS CASA C-295M [20]

The C-295M is a EADS CASA (now Airbus Military) twin-turboprop multi-mission aircraft developed by the former Construccionnes Aeronauticas SA (CASA), a founder member of EADS company based in Madrid. The aircraft is a stretched derivative of the CN-235 transporter and is noted for its short take-off and landing capability on semi-prepared runways and for the large payload capacity of 9250 kg. The landing and take-off run, of just 320 m and 670 m respectively, allow the aircraft access to runways close to operational or crisis areas or where supplies and troops are needed.

As case example of trending in twin-turboprop MP aircraft, international orders and delivery are described in a row[1].

A total of 208 C-295 aircraft have been ordered by 28 countries as of December 2018. Of this total, 168 aircraft have been delivered and 166 are in operation. The operators include Polish Air Force (17 deliveries complete),

[1]Market details are from an article on *Air Force Technology* [7]

UAE Navy (five for maritime patrol), Brazilian Air Force (15 to support the SIVAM Amazon monitoring project,13 aircraft are delivered as of January 2019), Swiss Air Force (two), Royal Jordanian Air Force (two deliveries completed), Algerian Air Force (six deliveries complete) and the Finnish Air Force (three deliveries complete), Egyptian Air Force (24 deliveries complete), Ghana (three deliveries complete), Ivory Coast (one), Mali Air Force (one), Bangladesh (one delivered), Indonesia (11 deliveries complete), Philippines Air Force (four deliveries of three aircraft complete), Thailand (Two – one aircraft delivered), Vietnam (three deliveries complete), Kazakhstan Air Defence Force (eight deliveries complete), Uzbekistan (four deliveries complete), Czech Republic (four deliveries complete), Portugal (12 deliveries complete), Spain (13 deliveries complete), Oman (eight deliveries complete), Saudi Arabia (four deliveries complete), Canada (16), Chile (three deliveries complete), Colombia (six deliveries complete), Ecuador (three deliveries completed), Mexico (14 deliveries completed).

In April 2005, Venezuela ordered ten C-295 transport aircraft, but the USA denied the export licence necessary for the American content of the aircraft and the order has been revoked. Portugal ordered 12 C-295 aircraft in February 2006, seven for military transport and five for maritime surveillance. Deliveries began in November 2008 and have been completed.

Poland ordered an additional two aircraft in October 2006 (delivered in September 2007) and two in October 2007 (to be delivered in 2009) to bring its fleet to 12 aircraft. Five more aircraft, worth $262m, were ordered in July 2012. The first two were delivered in October 2012 and the third in December 2012. The remaining aircraft were delivered by 2013.

In October 2007, the Chilean Navy purchased three aircraft. The Colombian Air Force ordered four aircraft in November 2007. The first two deliveries were made in June 2008, while the third and fourth were delivered in November 2008 and April 2009 respectively. Two more aircraft were ordered, one in September 2012 and the other in January 2013. Deliveries of all six aircraft are made.

The Czech Air Force ordered four C-295 aircraft in May 2009. Deliveries began at the end of 2009 and concluded in 2010. ADS CASA was teamed with Raytheon to offer the C-295 combined with the CN-235-300 for the US Army Air Force joint cargo aircraft (JCA) competition. The C-27J was chosen in June 2007.

In February 2012, Indonesia placed an order for nine C-295 aircraft. The first two were delivered to the Indonesian Air Force in September 2012. As of January 201, there are 11 C-295 aircraft operational with Indonesia.

In March 2012, Kazakhstan's Ministry of Defence placed an order for two aircraft. A Memorandum of Understanding (MoU) was also signed for six additional aircraft. Kazakhstan took delivery of the first two C295s in January 2013. All eight aircraft were delivered.

Airbus Military received an order from Oman in May 2012 for the delivery of C-295 aircraft in tactical transports (five) and maritime patrol aircraft (three) configurations. As of December 2018, all eight C-295 aircraft are in service.

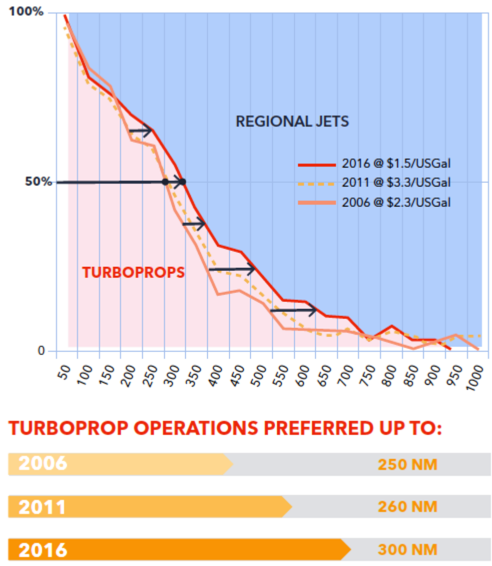

(a)

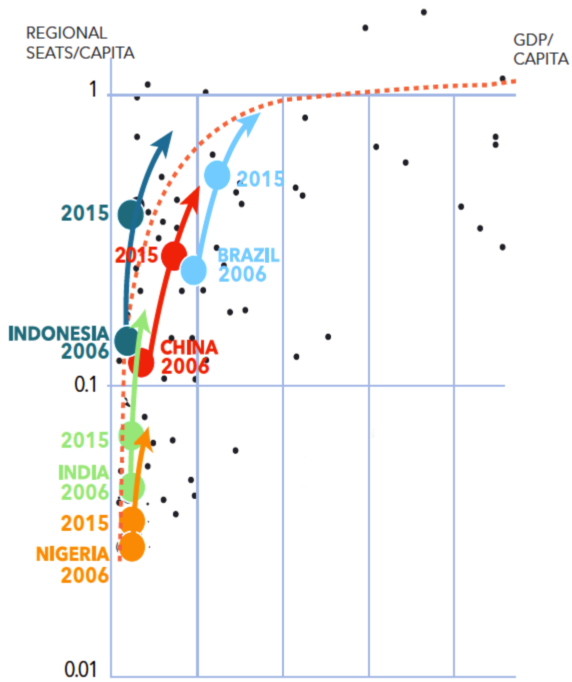

(b)

Figura 1.5: a) Turboprops have extended their operational scope over jets, proving to be the preferred airline choice for short haul operations [2]. b) Growth in regional seats per capita is correlated with country's wealth. As GDP per capita increases, the prospective for regional aviation drastically improves, especially when countries adopt regional air connectivity to accelerate economic growth [2].

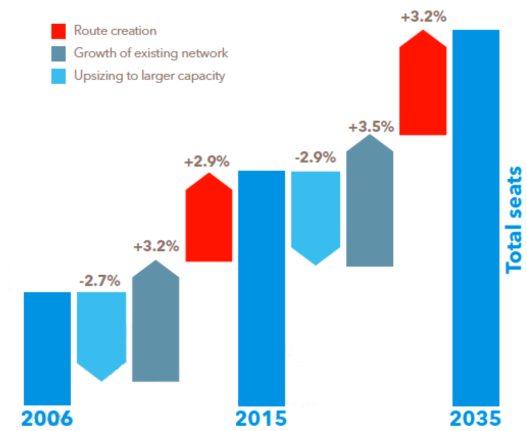

(a)

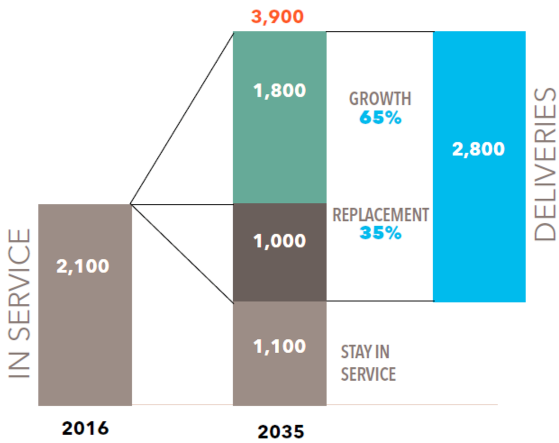

(b)

Figura 1.6: a) Classification of the average annual growth in turboprop market from 2006 to 2035. 50% of growth will come from route creation [2]. b) Forecast classification of turboprop fleet evolution and deliveries in 2035. It is expected an increase of 86% over the fleet is service [2].

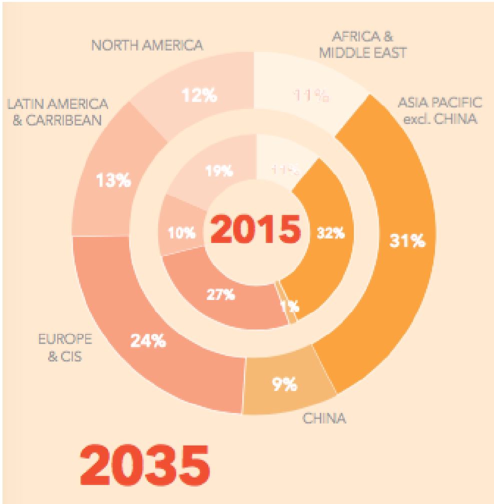

Figura 1.7: Actual and expected activity in turboprop's sector vary by region [2]

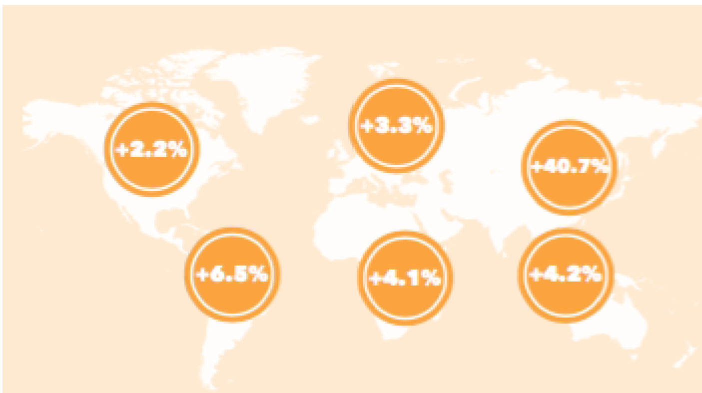

Figura 1.8: Turboprop in-service fleet evolution. Annual growth rate [2]

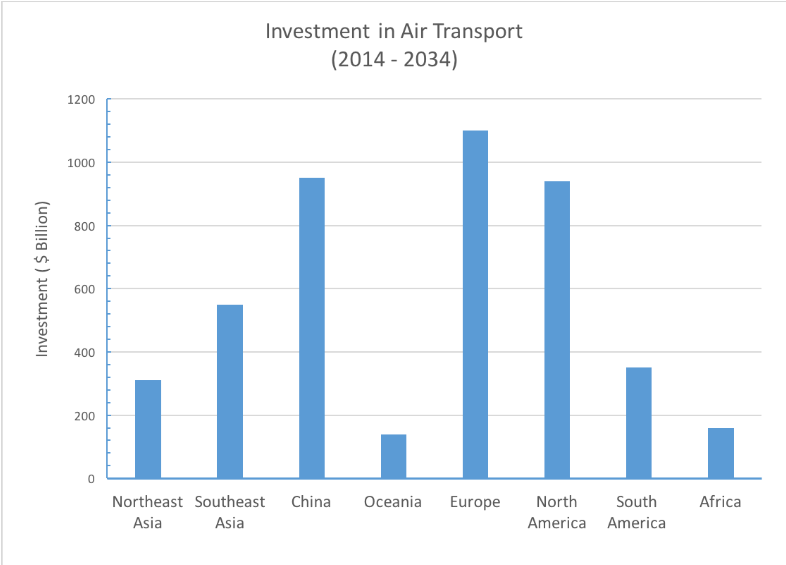

Figura 1.9: Investment in Air Transport vary by region

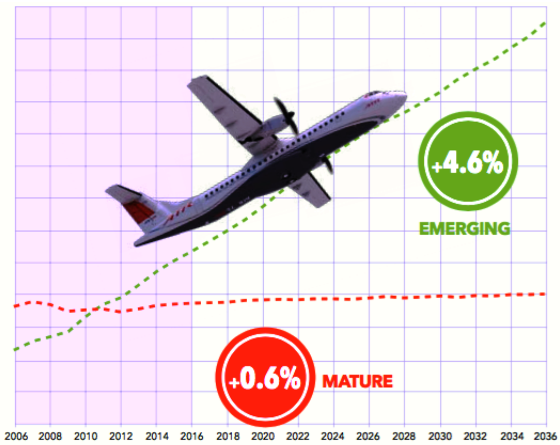

Figura 1.10: regional traffic demand comparison between mature and emerging economies. [2]

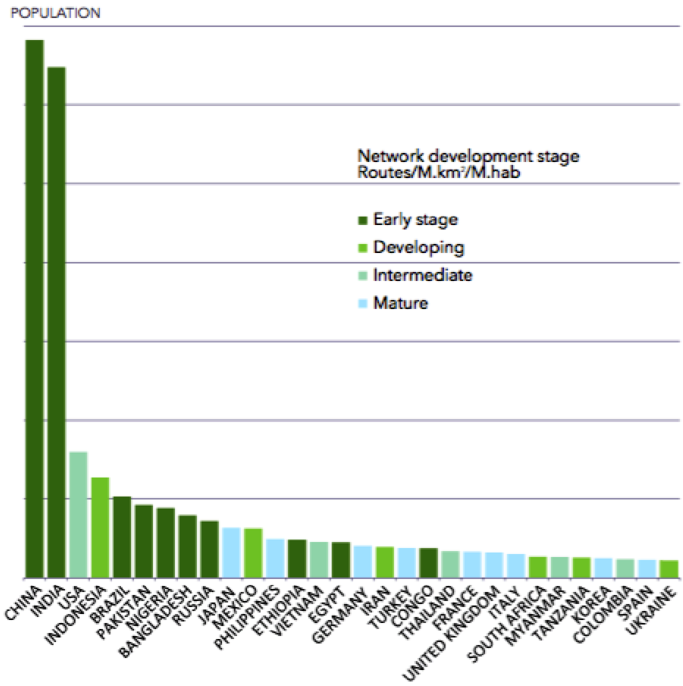

Figura 1.11: Network development by region [2]

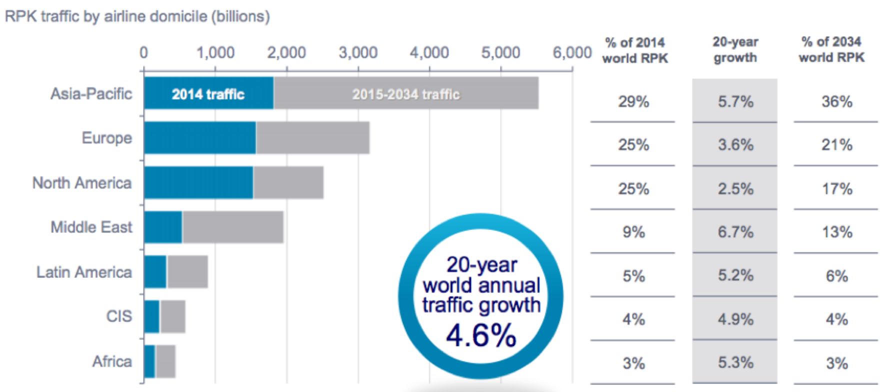

Figura 1.12: Northeast Asia market value [6]

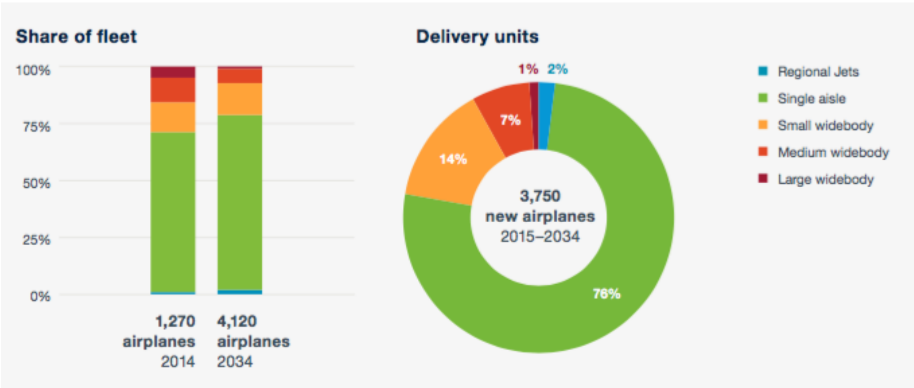

Figura 1.13: Southeast Asia market value [5]

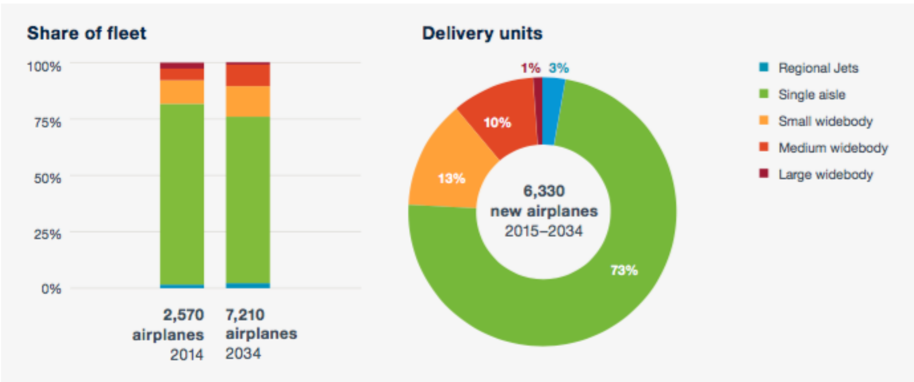

Figura 1.14: China market value [5]

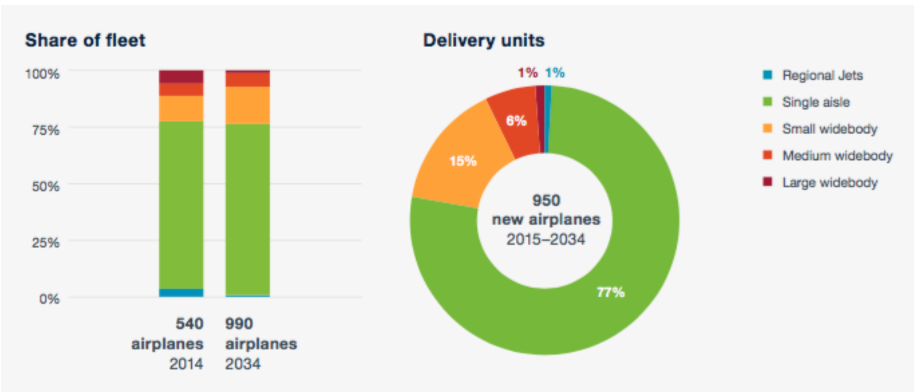

Figura 1.15: Oceania market value [5]

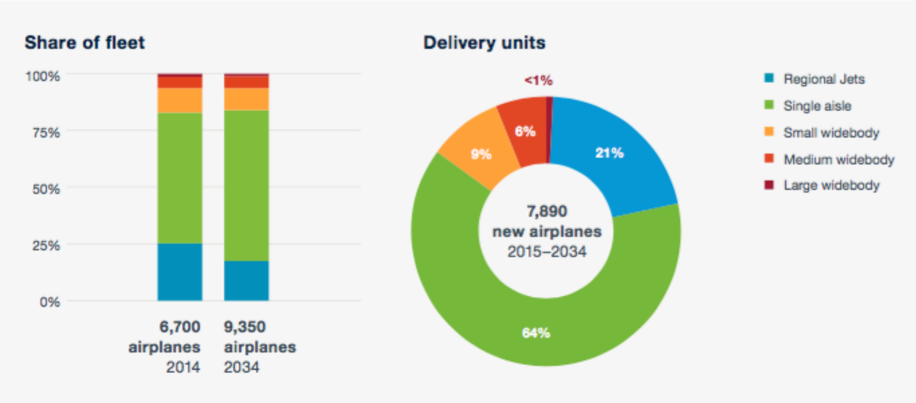

Figura 1.16: North America market value [5]

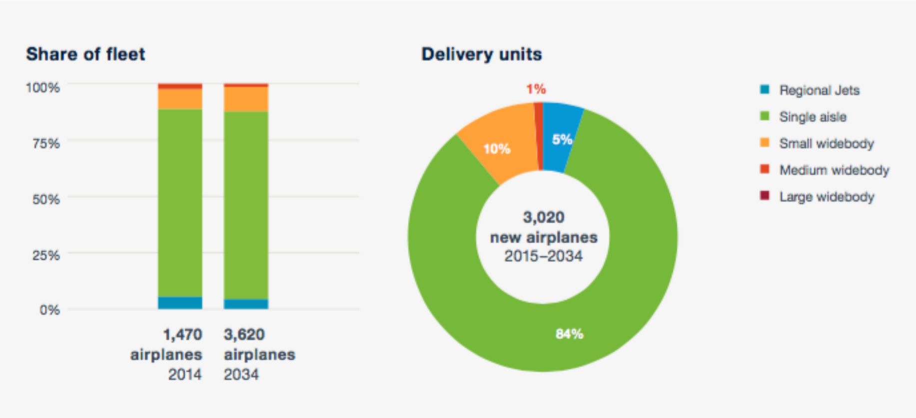

Figura 1.17: South America market value [5]

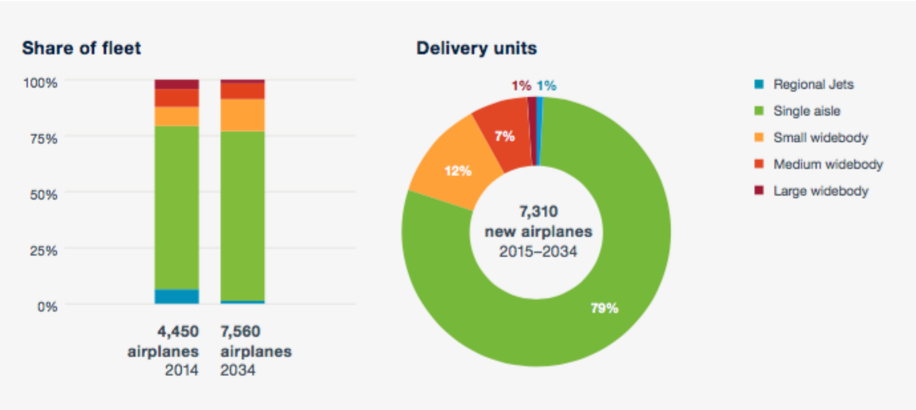

Figura 1.18: Europe market value [5]

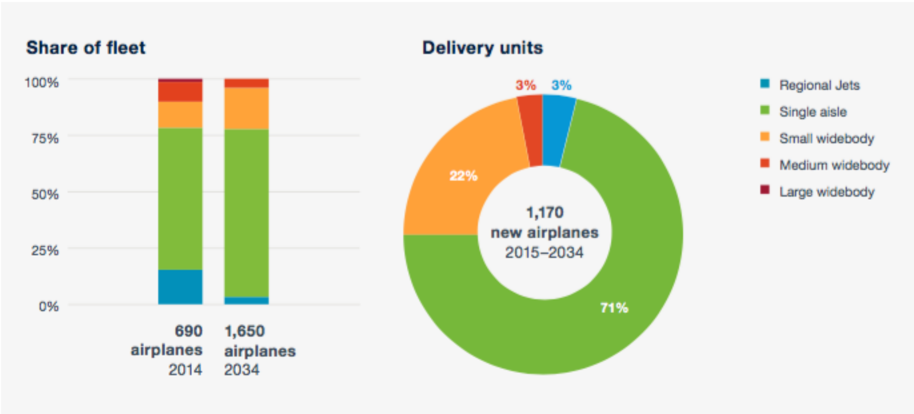

Figura 1.19: Africa market values [5]

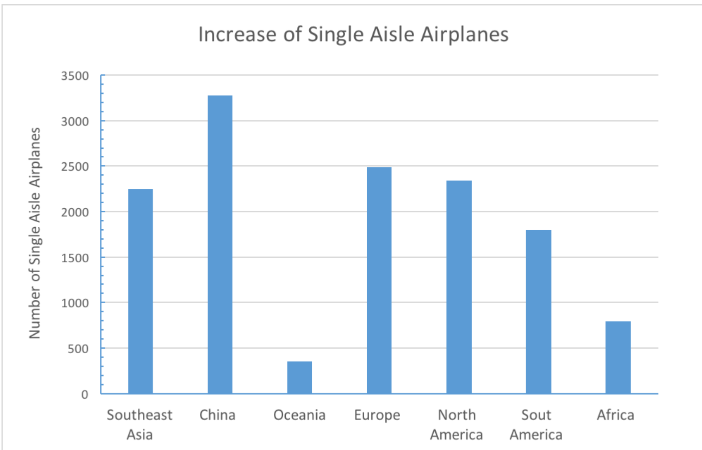

Figura 1.20: Increase of single aisle airplanes [5]

Capitolo 2

Reference Aircraft

The following section presents the reference aircraft on which the next section the statistical analysis was performed. They are shown in the various tables for the main characteristics similar to aircraft size and number of passengers.

2.1 ATR 72 MP

Figura 2.1

Characteristic	Value
Operators	8
Troops	70
Fully equipped paratroops	48
MTOW [kg]	23.000
Range [nm]	1.750
Power [shp]	2750 shp
Length	30,83
Wingspan	27,05

Tabella 2.1: Main characteristic of ATR 72 MP

2.2 C 27J - Spartan

Figura 2.2

Characteristic	Value
Operators	2+1
MTOW [kg]	31.800
Range [nm]	699
Power [shp]	5071 shp
Lenght	32,8
Wingspan	28,4

Tabella 2.2: Main characteristic of Q400

2.3 CASA CN-295 MP

Figura 2.3

Characteristic	Value
Operators	3
MTOW [kg]	23200
Range [nm]	2430
Power [shp]	2645 shp
Lenght	24,5
Wingspan	25,81

Tabella 2.3: Main characteristic of CASA CN-295 MP

2.4 EADS HC-144 Ocean Sentry

Figura 2.4

Characteristic	Value
Operators	6
MTOW [kg]	16502
Range [nm]	1801
Power [shp]	1807
Length [m]	21,41
Wingspan [m]	25,81

Tabella 2.4: Main characteristic of EADS HC-144 Ocean Sentry

2.5 HC - 130 Hercules

Figura 2.5

Characteristic	Value
Operators	7
MTOW [kg]	79379
Range [nm]	4500
Power [shp]	4300
Length [m]	34,37
Wingspan [m]	40,4

Tabella 2.5: Main characteristic of HC - 130 Hercules

Capitolo 3

Data Collection

One of the first phase of the *conceptual design* is to collect specifications from aircraft that can be get to grips whit the one we are going to plan. Obviously, there will be some differences between them, but we can make statistical analysis helping us have preliminary ideas on some data that opportunely correct will be the core of our project.

It's important to submit that even if the HC-130J has significant differences with the aircraft we are going to design, its presence in this sheet is justified by helping the statistical analysis.
This help obviously appear watching the trend line which characterise each plot in next section. This aircraft pefectly suits the trend line and we can use this property like taking the position of HC-130J as an infinite limits of the design.

3.1 Statistical analysis

In the last chapter, some reference aircraft have been presented. Their specifications are been collected and analysed in an Excel cartel so it has been possible to parallel them and extrapolate some starting points for the phase of *preliminary design*.

Very important is to note that for our purpose, having a classical approach is not useful.
According to literature [1], conceptual design requires for the statistical analysis phase to plot the specifications collected with the number of passengers that aircraft is design to.
This approach is obviously wrong for our application but, as the number of passengers represent the payload, we can use this specification as main characteristic.

The results from analysis will be shown in the next tables. In particular, will be presented the connection between:

- Fuselage length - payload;
- Fuselage height - payload;
- Wingspan - payload;

[1] [12], [13]

- Wing area - payload;
- Aspect Ratio - payload;
- Vertical Tail area - payload;
- Horizontal Tail area - payload;
- Shaft Horsepower - payload;
- MTOW - payload;
- OEW/MTOW - payload;
- Max Cruise Speed - payload
- Range - Payload;
- Range - MTOW.

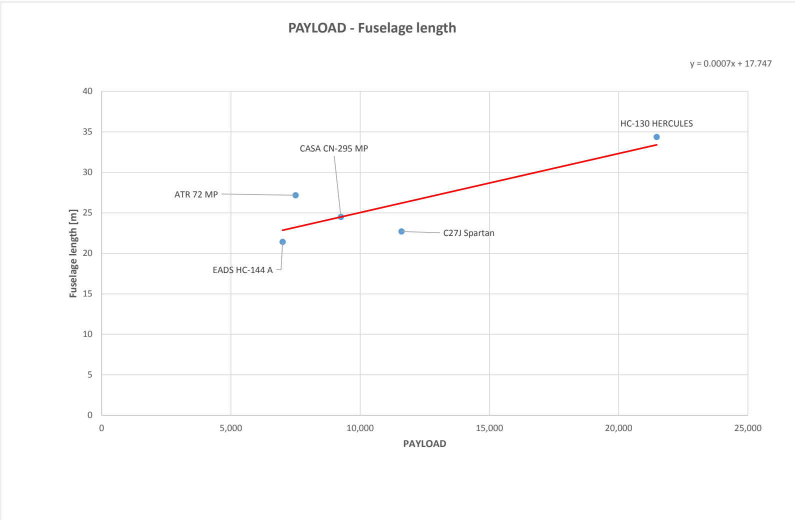

Figura 3.1

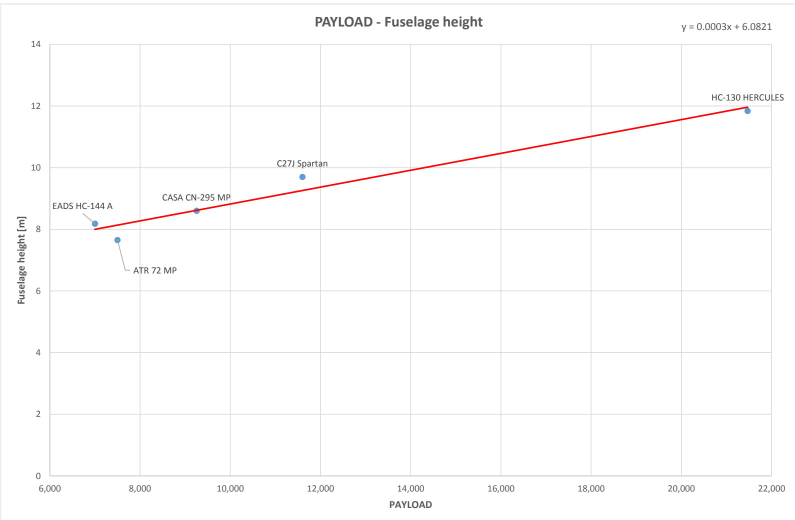

Figura 3.2

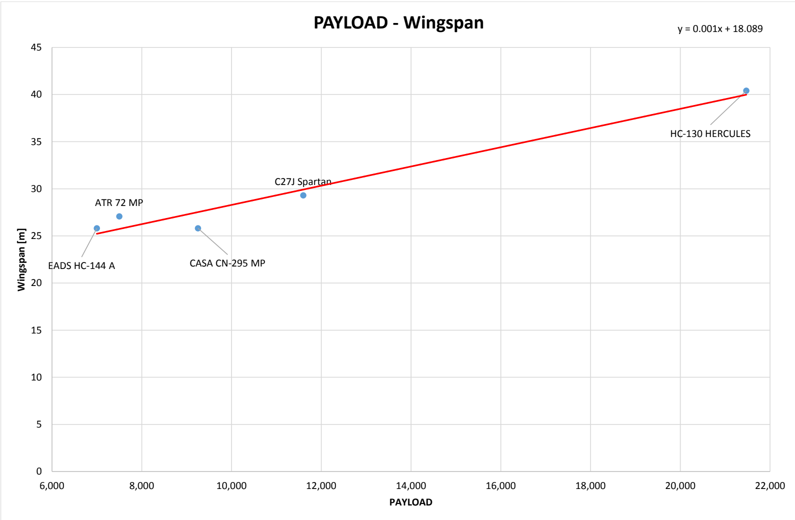

Figura 3.3

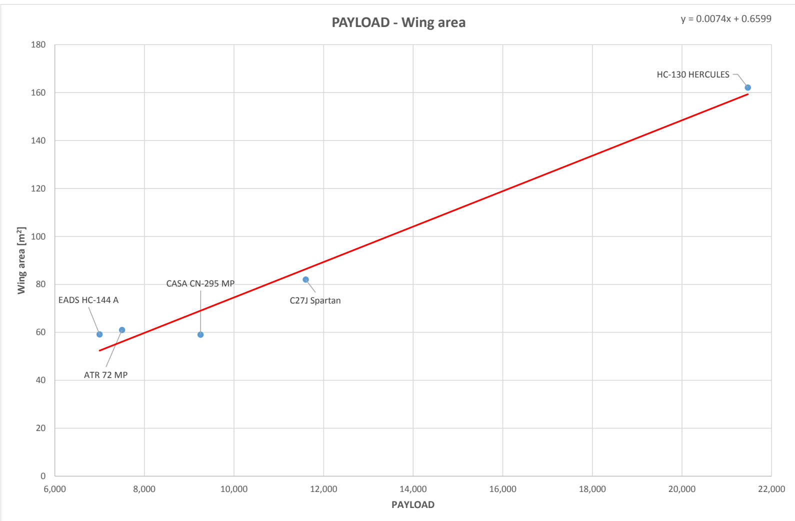

Figura 3.4

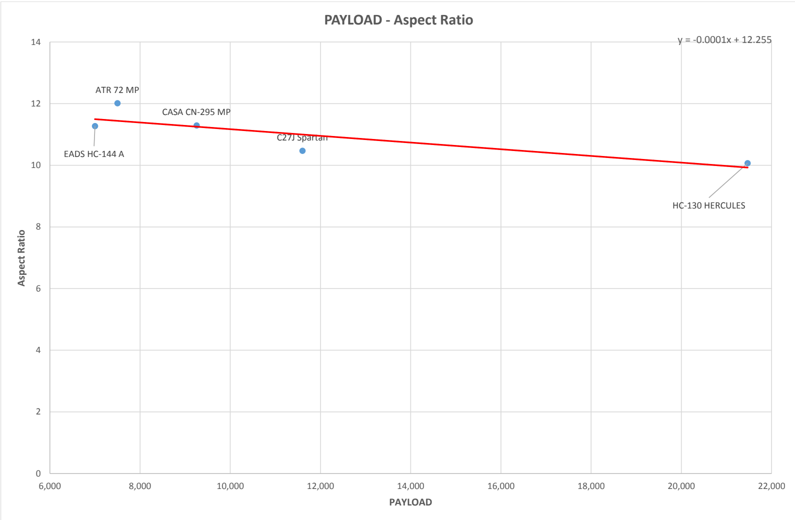

Figura 3.5

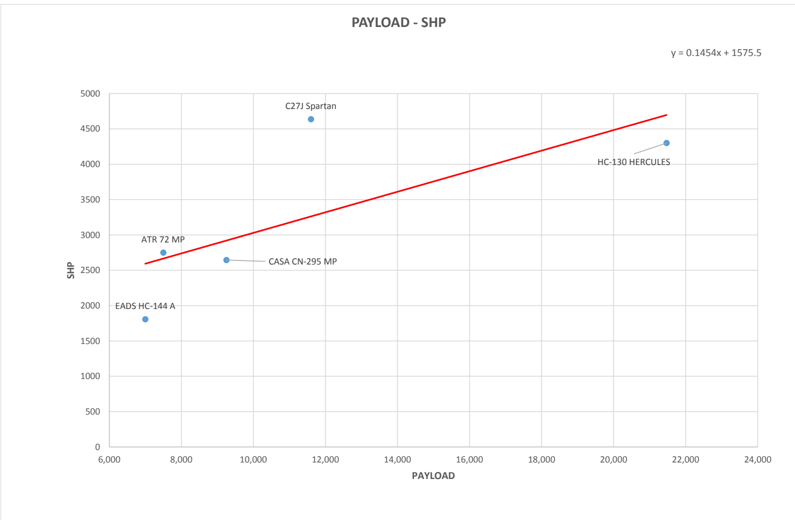

Figura 3.6

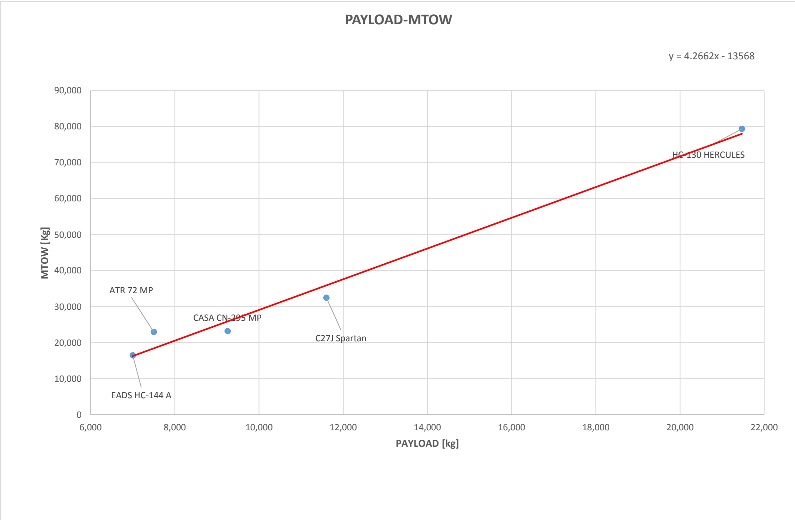

Figura 3.7

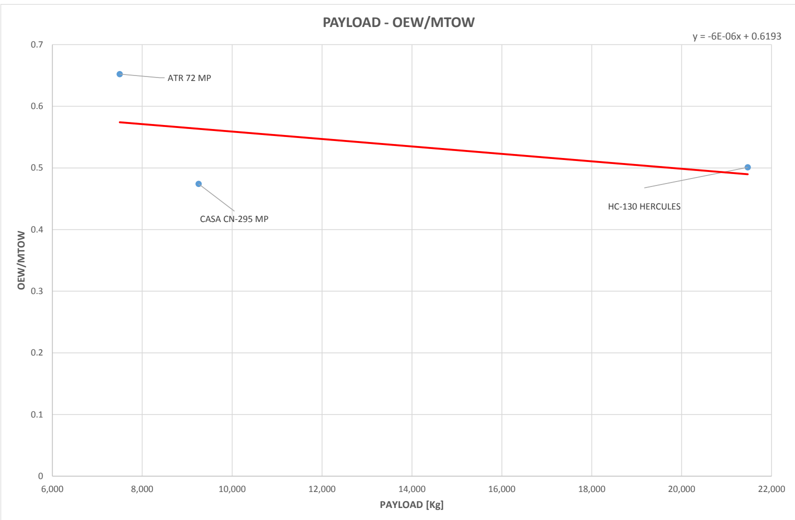

Figura 3.8

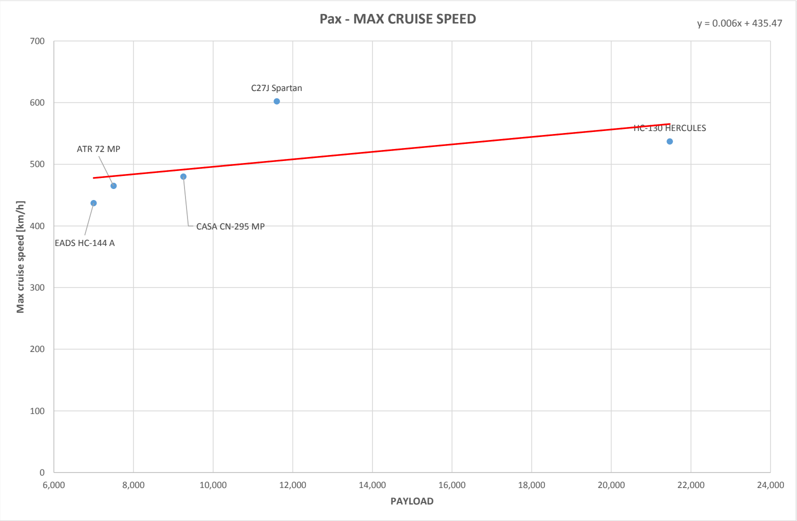

Figura 3.9

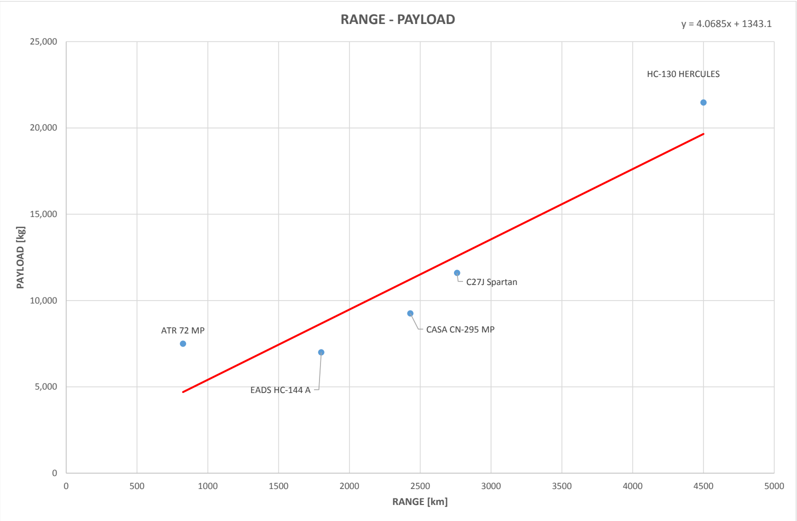

Figura 3.10

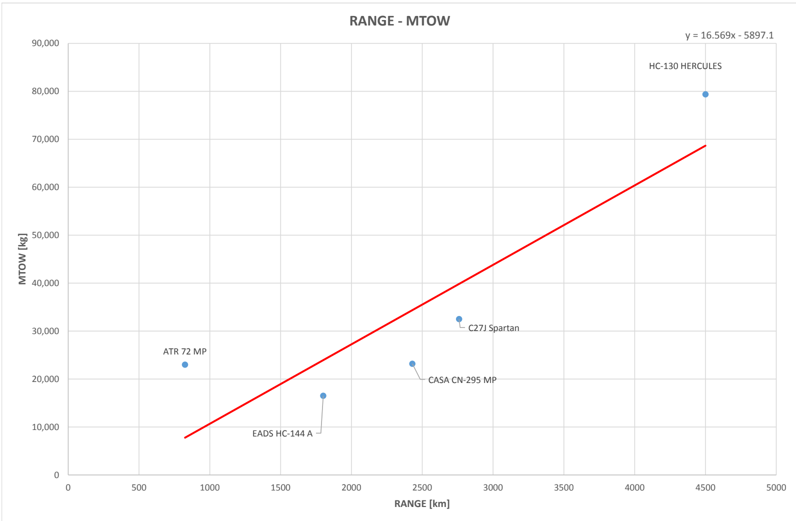

Figura 3.11

In view of all this, as a result of the linear regression and considering the project specifications it is possible to get some expected results for the aircraft we are going to plan:

- Fuselage length: $24.257\,m$;
- Aircraft height: $8.8721\,m$;
- Wingspan: $27.389\,m$;
- Wing Area: $69.4799\,m^2$;
- MTOW: $26107.66\,Kg$;
- OEW: $14711.66641\,Kg$.

Capitolo 4

Aerodynamic Analysis

From the previous data collected, in this chapter it is going to be developed the aerodynamic study of each surface of the airplane. To chose which profile will be the optimum for the turboprop, and taking into account the state of the art referred to the turboprop's airfoil used, it has been examined the following families[1]:

- NACA 24XX
- NACA 230XX
- NACA 44XX
- NACA 64XX
- NACA 250XX
- NACA 430XX

4.1 Airfoil Analysis

In order to collect data for the analysis, software like *XFOIL* and *Airfoils Tools* have been used to study different airfoils families. A viscous regime flow has been adopted in order to calculate the Reynold number, which value has been setted in $Re = 1e^7$. Such Reynolds number has been calculated by the equation below (eq.4.1), taking into account the following physics variables:

- density: $\rho = 0.4173 kg/m^3$ (because of $h_{cruise} = 8179 m^2$);
- cruise velocity: $V_{cruise} = 153,73 m/s$;
- cinematic density $\nu = 1.5214 \cdot 10^-5 kg/(m \cdot s)$ (computed by Sutherland's law);
- approximated chord ($c = 2.366m$).

[1] It's known that ATR-600 families have NACA 430XX serie as wing airfoils.[8]
[2] From Iso-Atmospheric tables.

$$Re = \frac{\rho \cdot c \cdot v}{\mu} \tag{4.1}$$

The values of dimensions and velocity from previous sections has been used for the analysis. Equally important is to note that a compressible regime in two dimensions has been setted. Considering, among other parameters, the structural and aerodynamic requirements, it has been implemented an airfoil with a 15% of thickness at the root and another one of 12% at the nearest sections to the tip. The results from the 2D analysis were exported from XFOIL (slightly modifying the file '.dat '),and loaded to Matlab (file named 'xfoil_data_airfoil.m'), where it was performed a comparison between them (after load and managed all the data correctly).

To be able to chose the right profile, first of all it has been obtained the geometry variables (area, thickness, camber, and angle of attack) of each one, and as a second step it has been computed the values of α, C_L, C_D, Efficiency. In the following five figures are shown one airfoil of each family elected (mentioned at the beginning of this section):

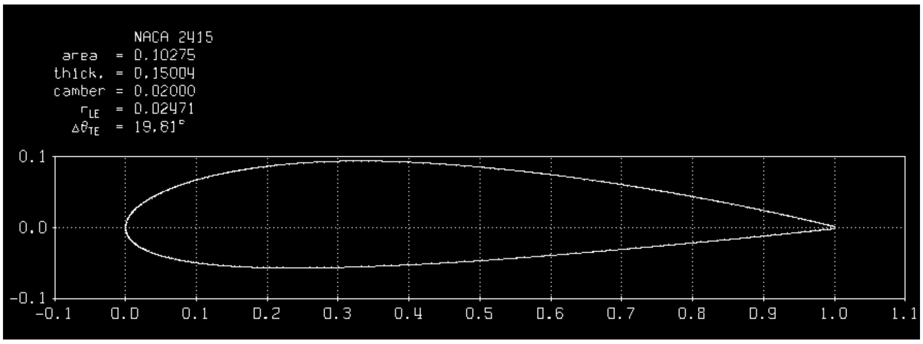

Figura 4.1: Geometry of NACA 2415

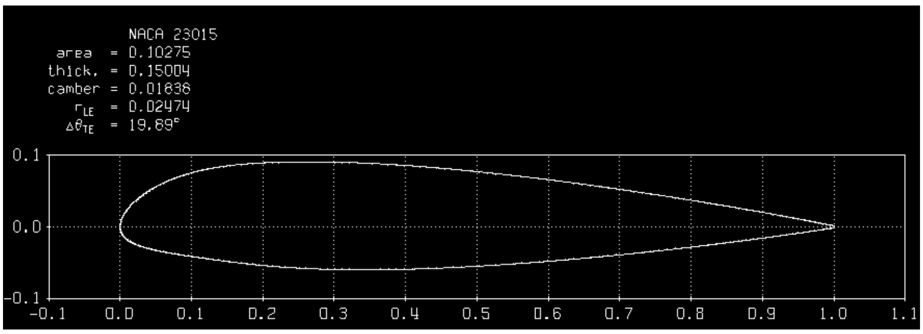

Figura 4.2: Geometry of NACA 23015

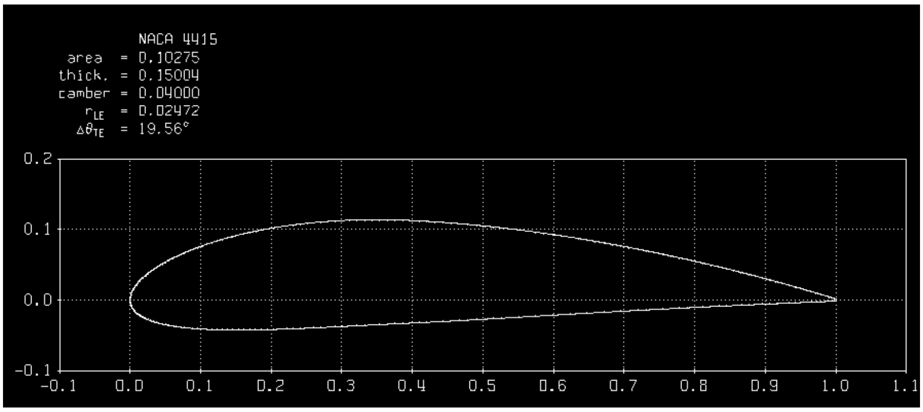

Figura 4.3: Geometry of NACA 4415

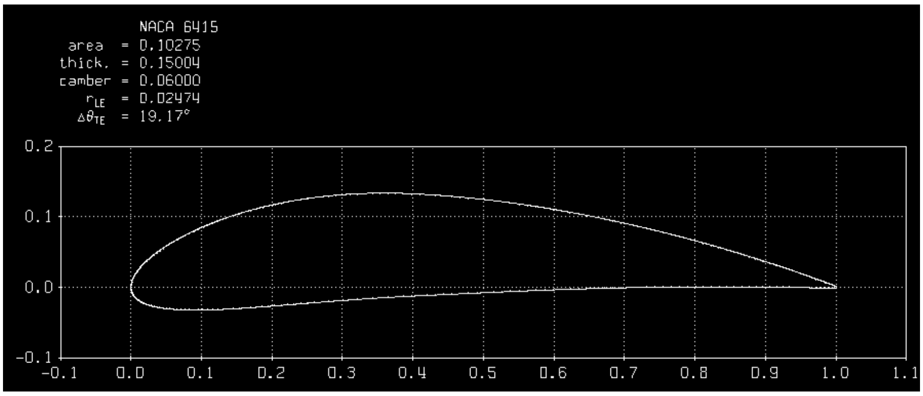

Figura 4.4: Geometry of NACA 6415

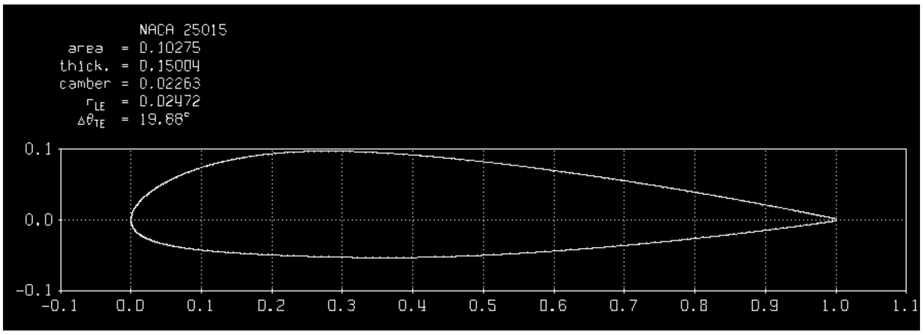

Figura 4.5: Geometry of NACA 25015

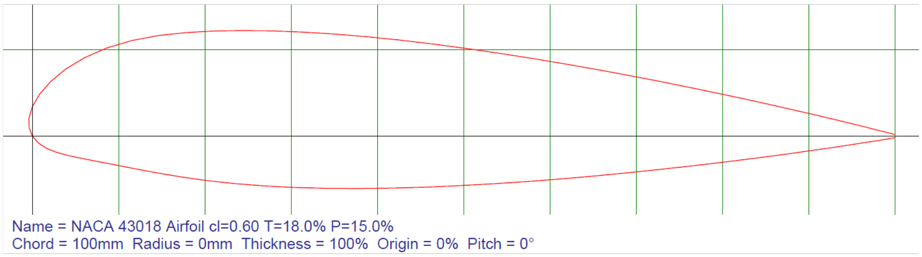

Figura 4.6: Geometry of NACA 43018

After considering the plots of: Cl - Alpha, Efficiency - Alpha and Polar curves (see the three figures below), the following conclusions were being achieved:

- The high efficiency, around $\alpha = 5°$ is obtained by the family NACA 44XX. This value of alpha is a common number for cruise.
- The polar curve of the family NACA 44XX have a better behavior compared to the others.
- Approaching the Cl - Alpha curve, NACA 44XX have a high C_{lMAX}, and at the same time it has a gradual decrease after the pick, that it mean an smooth boundary layer separation.

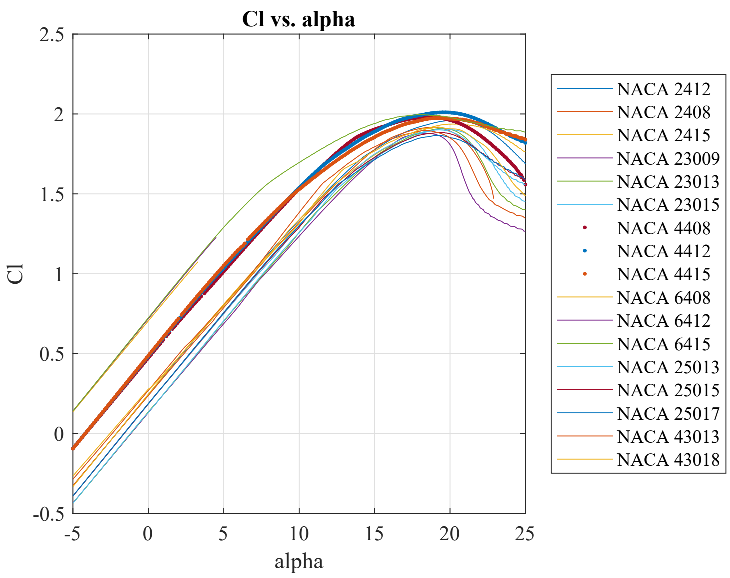

Figura 4.7: Curves of Cl - Alpha of each studied airfoil

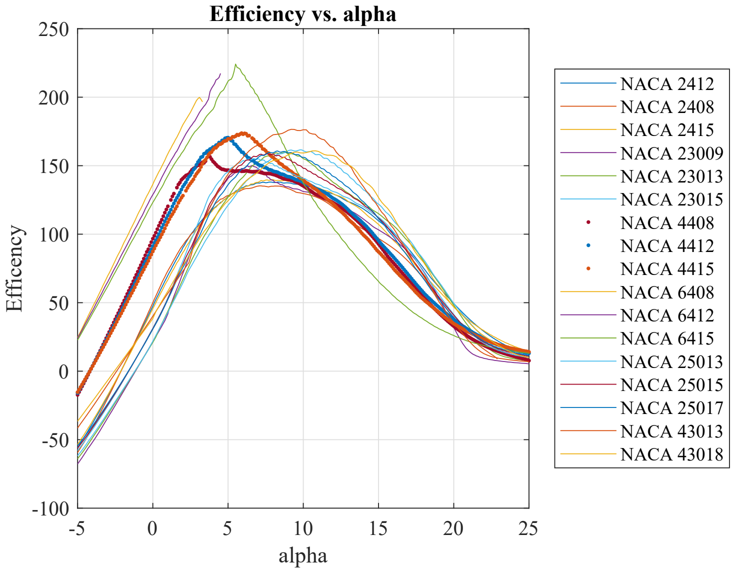

Figura 4.8: Curves of efficency - Alpha for each studied airfoil

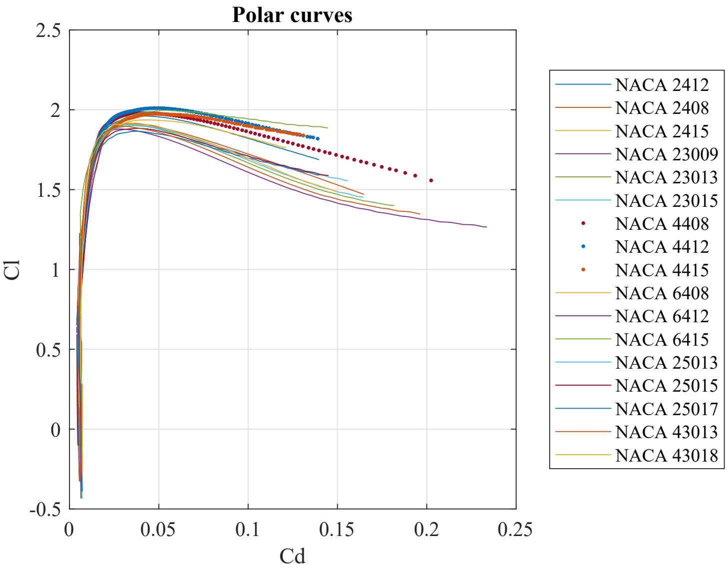

Figura 4.9: Polar curves of each studied airfoil

For all these reasons mentioned before, the selected airfoils for the wing are NACA 4415 at the root's zone and NACA 4412 at the tip's zone.

4.2 Wing Analysis

After choosing the two airfoils which will constituted the wing, several wing geometries have been design (always trying to be in the same 'wing concept' of turboprops' group), and the final design of the wing is shown in the following figure:

Figura 4.10: Geometry of the wing

Finally, it could be obtained the polar curve and have the aerodynamic contribution of the wing, as it is illustrated in the following figures. All the results have been computed by the 'wing_design.m' file attached in the project.

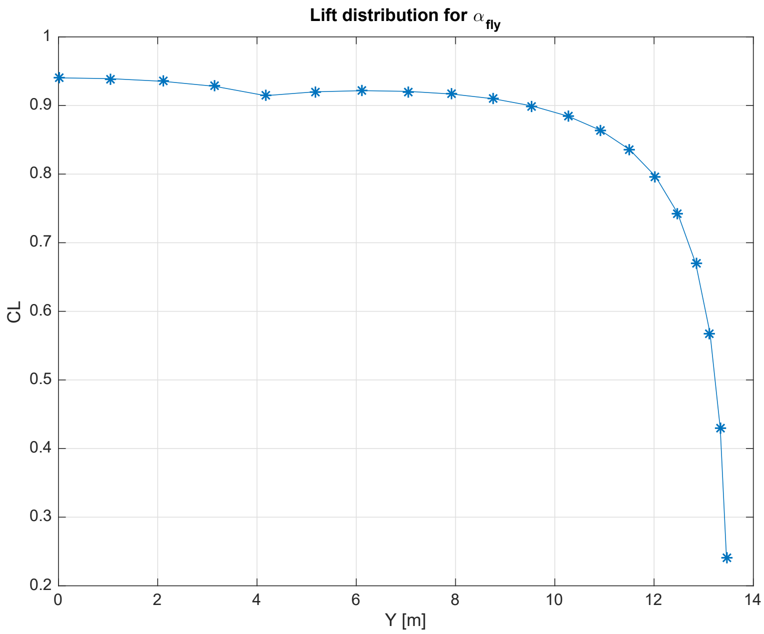

Figura 4.11: Curves of Cl - Alpha of the wing

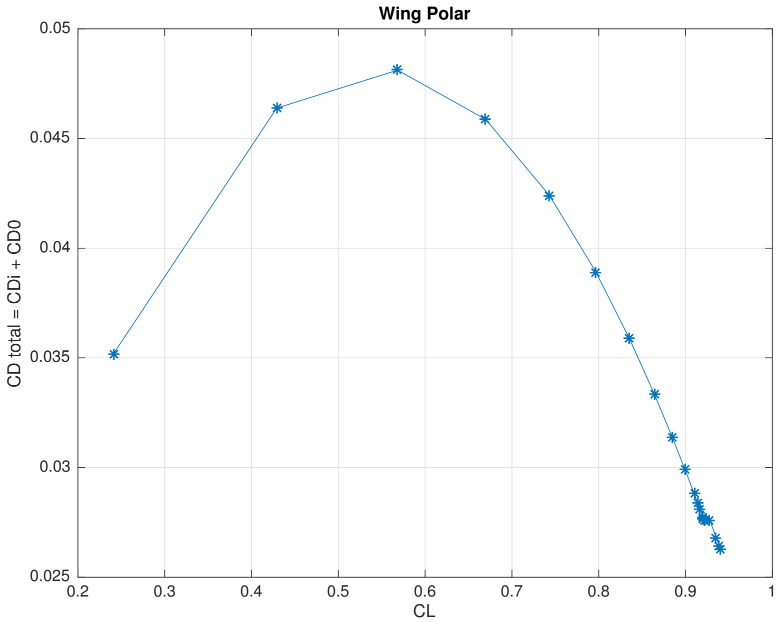

Figura 4.12: Polar curves of the wing

After testing different combinations and knowing these statements the wing was designed:

- A high value of the efficiency is required in order to decrease the consumption of the aircraft.
- If was only taken into account the first point, anyone would though about building an elliptic wing, but in this point appears the cost of the product, which assumes an important role in the project. Because of that, a simple and easy-building wing should be chosen.
- Furthermore, it is important to achieve a cross between the velocity of cruise and the value of the drag.

The final geometrical values of the wing are specified in the following table:

Characteristic	Value
Wingspan $[m]$	27
Wing surface $[m^2]$	62.686
Incidence alpha [°]	5
Tip chord $[m]$	1.41
Root chord $[m]$	2.54
Taper ratio	0.551
Aspect ratio	11.6294

Tabella 4.1: Geometrical wing characteristics

It is important to note that on the basis of considerations below iteration by iteration we have decrease the value of wing surface chosen as starting value to increase the aspect ratio in reason to get closer to an elliptic wing.
The final values of C_L, C_D, C_{D0}, E and e (Oswald's factor) are shown in the following table:

Characteristic	Value
C_L	0.8627
C_D	0.0284
C_{D0}	0.001071
C_{Di}	0.0208
Efficiency	30.3715
Oswald's factor	0.9800

Tabella 4.2: Aerodynamic wing characteristics

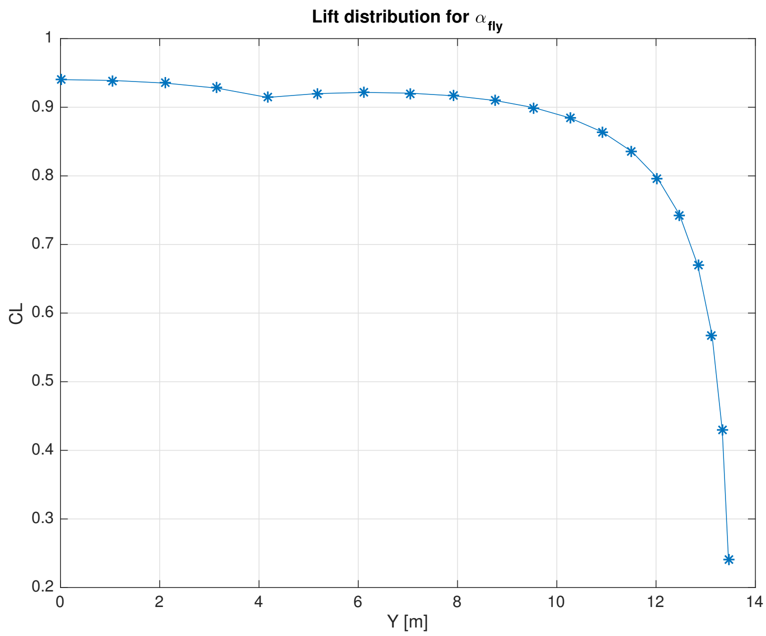

Figura 4.13: Distribution of the lift along the wing

4.3 Analysis of the Horizontal and Vertical Stabilizer

The analysis of the horizontal stabilizer follows the same steps (every line in Matlab files has his description of what is being done) as the wing's procedure, using 'v_stabilizer_design.m' and 'h_stabilizer_design.m' files attached in the project too. It should be highlighted that for the vertical stabilizer (rudder), it was only required to calculate the lift-induced drag, while for the horizontal stabilizer (elevator), it was necessary to repeat the same process executed for the wing. The airfoil used for the rudder is NACA 0010, on the other hand, for the elevator it has been utilized NACA 0012.

The geometry of the rudder and elevator is appreciable in the next two figures:

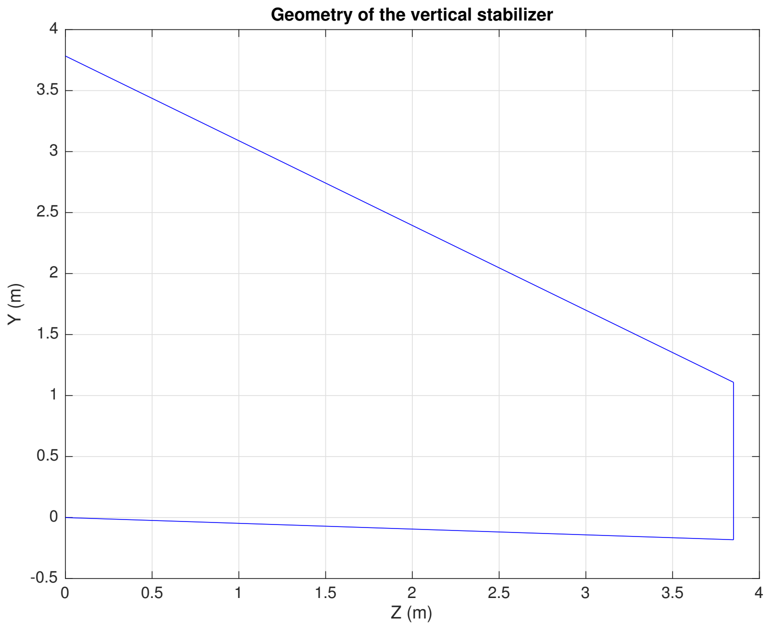

Figura 4.14: Definition of the vertical stabilizer's geometry

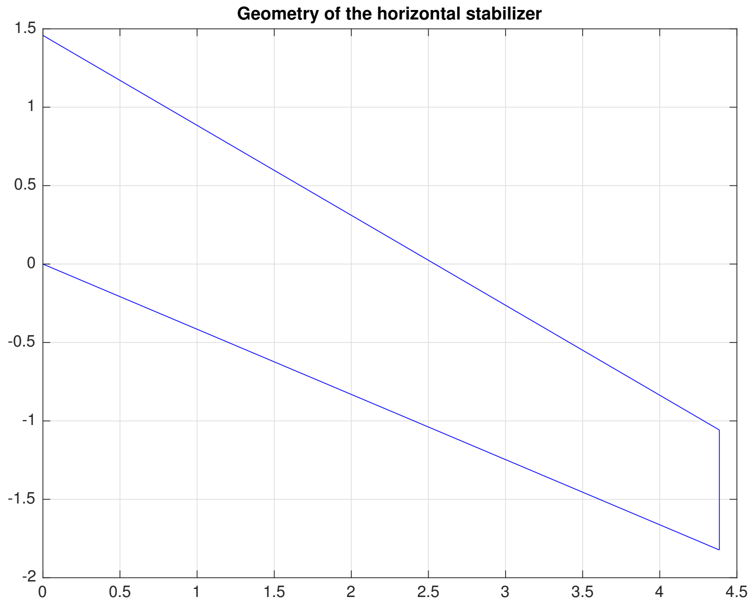

Figura 4.15: Definition of the horizontal stabilizer's geometry

In addition are being defined the principle characteristics of the two surfaces:

Characteristic	Value
C_L	-0.02688
C_{Di}	0.00008
C_{D0}	0.00227
Oswald's factor	0.6971

Tabella 4.3: Aerodynamic elevator characteristics

Characteristic	Value
C_L	0
C_{Di}	0
C_{D0}	0.0026

Tabella 4.4: Aerodynamic rudder characteristics

4.4 Analysis of the Drag

To determine the total drag of the aircraft is necessary to consider: wing, fuselage, tail and nacelle. The total coefficient of the drag will be formed by: parasitic drag, induced drag, wave drag, interference drag. To be able to complete the study it was required several geometric data. In addition should be added that the nacelle has been approximated to a cylinder, and also the front part of the fuselage, while the nose and tail sections have been taken as cones. The calculation of the wet surface was also performed before analyze any type of drag.

4.4.1 Parasitic Drag

The parasitic drag is defined as:

$$C_{D0} = \sum C_f \cdot F \cdot Q \cdot [S_{wet}/S_{ref}] \tag{4.2}$$

Where C_f is the friction coefficient, F is the form factor, Q is the interference factor, S_{wet} is the wet surface and S_{ref} is the reference surface. Knowing that the Reynolds number is high, the C_f is calculated for the different surfaces in turbulent flow as:

$$C_F = \frac{0.455}{[(logRe_c)^2.58(1+0.144M^2)^0.65]} \tag{4.3}$$

The form factor, F, is calculated in different ways: Wing:

$$C_{Fw} = 3.3758e - 4 \tag{4.4}$$

$$F* = 1.5859 \tag{4.5}$$

$$Q = 1 \tag{4.6}$$

Tail:

$$C_{F\ tail} = 3.6938e - 4 \tag{4.7}$$

$$F* = 1.3520 \tag{4.8}$$

$$Q = 1.2 \tag{4.9}$$

Fuselage:

$$CF_fus = 3.3296e - 4 \tag{4.10}$$

$$F* = 1.0650 \tag{4.11}$$

$$FQ = 1.25 \tag{4.12}$$

Nacelle:

$$CF_nac = 4.1161e - 4 \tag{4.13}$$

$$FQ_nac = 1.25 \tag{4.14}$$

At the end, the values of each element contributing to the parasite drag are:

4.4.2 Induced Drag

The induced drag it was already calculated int the previous sections, although in the following table are expressed the exact values for the wing and the horizontal tail:

Characteristic	Value
C_{D0} wing	0.001071
C_{D0} tail	0.000360
C_{D0} fuselage	0.001416
C_{D0} nacelle	0.000048
C_{D0} TOTAL	0.002895

Tabella 4.5: C_{D0} contribution of each component

Characteristic	Value
C_{Di} wing	0.0208
C_{Di} horizontal tail	$8e^{-5}$
C_{Di} total	0.0209

Tabella 4.6: C_{Di} contributions

4.4.3 Wave Drag

The wave drag is the component of the aerodynamic drag due to the presence of the shock waves. From the wing's characteristics is possible to extract:

$$M_{crit} = M_{dd} - (0.1/80)^1/3M_{dd} = k_a/cos(\Lambda) - (t/a)/cos^2(\Lambda) - C_L/(10cos^3(\Lambda)) = 0.7164 \tag{4.15}$$

If the Mach$_{cruise}$ number is higher than the critical one, then it will be possible to calculate the wave drag as:

$$C_{Dwave} = 20(M - M_{crit})^4(S_{strip}/S_{ref}) \tag{4.16}$$

In the following table are expressed the exact values of this parameter:

Characteristic	Value
k_a	0.95
S_{strip}	31.3430
M_{cruise}	0.5003
M_{dd}	0.7164
M_{crit}	0.6087
C_{Dwave}	0.0014

Tabella 4.7: C_{Dwave} contributions

4.4.4 Interference Drag

This component of the drag is generated for the interference between the fuselage and the lift surfaces. Is it possible to calculate it as:

$$CD_{inter} = 17(t/c)^4 - 0.05(t/c)^2\frac{c^2}{S_{ref}} \tag{4.17}$$

In the following table are expressed the exact values of this parameter:

Characteristic	Value
k_a	0.95
$C_{Dstruct}$ wing	0.0015
$C_{Dstruct}$ horizontal stabilizer	$3.8998e^{-5}$
$C_{Dstruct}$ TOTAL	0.0016

Tabella 4.8: $C_{Dstruct}$ contributions

Characteristic	Value
C_{D0} Total	0.0029
C_{Di} Total	0.0209
$C_{Dstruct}$	0.0016
C_{Dwave}	0.0014
C_D TOTAL	0.0267

Tabella 4.9: C_D TOTAL contributions

After compute all the diverse drag contributions is observed how the wing and the induced drag are the main creators of drag, as it could be seen in the following table:

At the end, it is possible to calculate the effective efficiency of the aircraft (in the previous chapters it has been calculated the effective efficiency of the isolated wing), using the C_D TOTAL as the pre-called C_{Dwing}:

Characteristic	Value
C_L	0.8358
C_L correction	
C_D	0.026737
E	31.2601

Tabella 4.10: Results of the drag

As it could be seen in the file drag_total_aircraft.m, the values of the wing's drag parasite coefficient were recalculated, for this reason the C_D of the total aircraft has achieved a roughly low value after made it. It should be said, as it was already expressed in other sections of the project, that aircraft design requires iterations to be optimal (by an engineering point of view).

4.5 Analysis of hyperlift devices

This chapter is merely focused in the qualitative point of view about the impact of devices which increase the lift, specifically flaps. Using the XFOIL program, it has been recalculated the coefficients of lift and drag with the airfoil NACA 4415 with a deflexion angle of 10°. The following picture shows the aspect of the configuration before performing the analysis:

Taking into account that the landing speed would be around 70 m/s (which changes the Reynolds number, and with it the XFOIL data should be computed again), the graphic comparison between the two airfoils are:

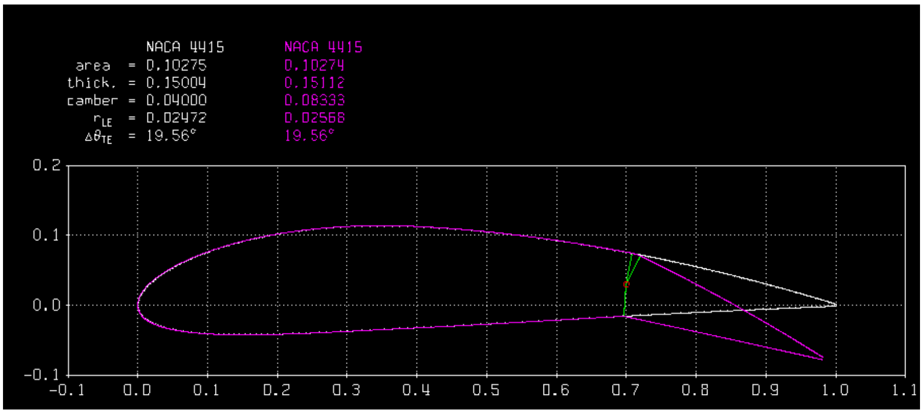

Figura 4.16: Geometry of NACA 4415 with 10° flap deflexion

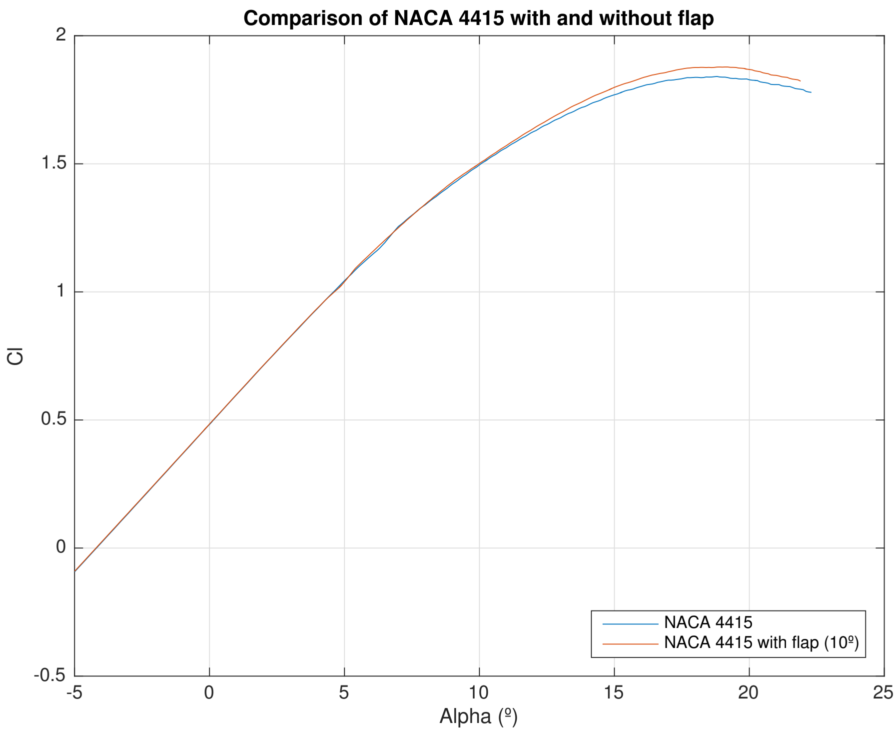

Figura 4.17: Comparison of the airfoil with and without flap

For this new study, that it should be said that was only considered the airfoil (not extrapolate to the wing), the results of the maximum lift coefficient are the following:

The procedure applied to obtain the results is saved inside the folder of 'flap analysis' together with the files .dat of each airfoil.

To sum up, as it was expected, flaps are used to increase the lift of an aircraft

Characteristic	Value
C_L NACA 4415	1.841
C_L NACA 4414 with flap	1.878
$Increase(\%)$	2.01

Tabella 4.11: Results of the drag

wing at a given airspeed, lowering the minimum speed at which the aircraft can be safely flown, and increasing the angle of descent for landing. In subsequent studies a deeply research of the kind of flap and the surface that it must have, it should be done to improve the performances of the turboprop.

Capitolo 5

Fuselage layout

In order to design the fuselage, from data collection we have got reference dimensions which have been used as first step for the iterations that have lead us to the final configuration.
It is important to note that in order to implement this phase of the project, several civil aircrafts have been studied. This choice may seem strange but we have to take into account that the majority of multirole maritime patrol aircrafts are a derivative of commercials ones.
On the other hand, even if the specification for a military aircraft may appear to be similar to that of a civil transport, including parameters such as design payload, design range, etc., the method by which some of these parameters, specifically the design payload, are determined is very different. For a civil transport aircraft, the payload is primarily passengers which are regularly arranged in a fuselage, often of cylindrical cross-section to minimise weight, whereas the payload for a militarist's varies in both shape and weight[1].

Another consideration is that a major requirement for any military aircraft is that of being able to load and unload any possible payload quickly, preferably with little or no extra handling systems to those available on the aircraft. This means that obviously the the floor of the cargo have to be hold as close to the ground as possible. Such a request can be fulfilled by adopting a high-wing configuration with undercarriage-mounted to the fuselage sides.

After this considerations have been made, we have started the procedure to dimensioning the fuselage.

5.1 Crew

In addiction to the Pilot and the Co-Pilot, we have to consider the presence of the operators that are needed to fully exploit the mission systems. Looking at the type of mission this aircraft is going to perform, we need three mission system operators:

- 2 on the modular mission suite which manages the aircraft wide array of sensors;

[1][13]

- 1 as observer with the main tasks of exploiting the aircraft bubble window to perform visual search and airdrop of emergency equipment through the aircraft in-flight operable door in the frame of *Search And Rescue* missions.

5.2 Toilettes

Considering that there are no specifically requirement for a military aircraft about having or not installed toilettes on board, it is important to note that on long-range aircrafts, excluding bombers, have the same systems used in their commercial counterparts.
Taking into account the number of operators on the aircraft, have been chosen to install 1 toilette in front af the cabin. According to JAR-25, toilette is 36 *in* width.

5.3 Doors and windows

5.3.1 Doors

Considering the requirement for an aircraft which have to perform SaR and MP, we need a *Crew entrance door* and a wide rear door with opening ramp.
As the dimension of the second one have a strictly dependance on types of cargo loads which have to be easily loaded, the *Crew entrance door* have to respond at specific requirements.
According to the JAR, we have installed 1 door *Type I*. This type is a floor level exit with a rectangular opening of not less than 24 inches (609.6 mm) wide by 48 inches (1,219 m) high, with comer radii not greater than one-third the width of the exit.

In order to promote competitiveness of the aircraft, a solution to accommodate fully equipped paratroop has been studied. Recently ATR has conducted an air experimentation proving that it is possible dropping paratroopers from a door installed on the back of the fuselage.
For these reasons we have installed a large door on the back, which dimensions are similar to the Type I door.

5.3.2 Windows

This aircraft has been design with the concept of windowless fuselage. This is a common characteristic for a military aircraft which doesn't need to accommodate operators comfortably.
However it is important to note that aircraft without windows are studied for the next generation of civil aircraft as a new revolutionary solution in the layout of the fuselage. In fact, projecting aircraft without windows will allow engineers to study lighter structures increasing at the same time safe. More pertinently, the absence of windows will reduce the weight of the aircraft – the insertion of windows requires additional structural supports and parts – and will lessen drag, thus diminishing travel times and fuel costs.
One of the most important centre for the research and technology of UK, the CPI (Centre for Process Innovation), presented an aircraft design where in place

Aircraft	With windows	Windowless
Boeing 767	86070 $[Kg]$ EW	84260 $[kg]$ EW
Lockheed $C-130$ Hercules	34274 $[kg]$ EW	35210 $[kg]$ EW
Casa $C-295$	23200 $[kg]$ $MTOW$	21000 $[kg]$ $MTOW$

Tabella 5.1: Differences in weights for the same aircraft with windows and windowless. The Lockheed C-130 with windows is the L-100.

of windows, the jet's interior walls was covered by thin display screens. Cameras on the exterior of the aircraft were able to transmit footage of the surrounding panoramas. Alternatively the screens could be used to show films or preloaded slideshows of calming images, or to display spreadsheets and work documents for meetings in the air.

In terms of weight, the difference between the two configuration (with and without windows) can be studied considering data weights collected taking into account three different aircraft: the Boeing 767, the Casa C-295 and the Lockheed C-130. All these aircraft have a civilian configuration with windows and a military configuration without windows. Differences in weights are shown in Tab.5.1

As we can see there is a margin of 1000-2000 kg for each aircraft that means a reduce of weight of 2.32% for the Boeing 767 and an 8.9% for the Casa C-295.

Another way to analys this configuration is taking into account the direct operative costs (DOC).
Under the DOC category all the costs associated with flying and direct maintenance must be considered (fig.5.1), however some standardised methods do not include all the factors.

DOC are determinate considering two models:

- The model studied by the associations of European airlines (normative AEA[2]);
- Model DAPCA IV (Development And Procurement Costs of Aircraft) elaborated by RAND Corporation and reported in [9].

According to those models, DOC can be evaluated by the eq.5.1

$$DOC = \frac{A + C + M}{P} \tag{5.1}$$

where:

- A is annual cost considering aircraft propriety;
- C is flight cost;
- M is the maintenance cost;

[2] [?]

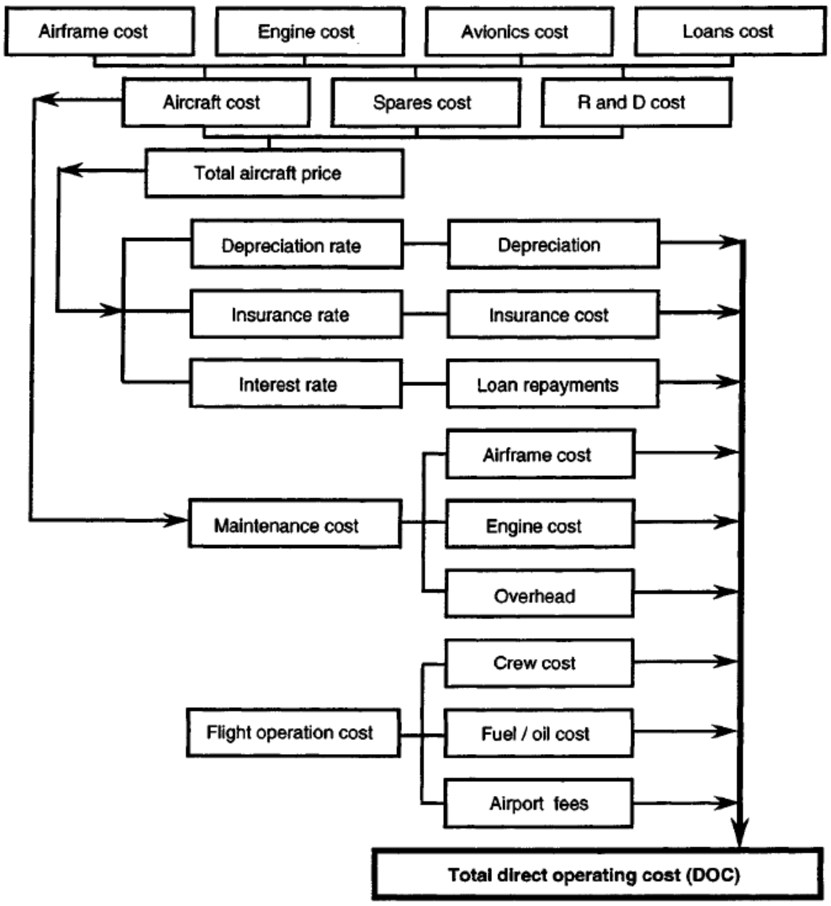

Figura 5.1: Direct operating cost components [13].

- P is the annual aircraft productivity which is the product of annual utilization, Commercial speed and number of passengers.

This four factor have a linear dependence with travel time, fuel cost, airframe maintenance cost and operative empty weight.

So the Windowless configuration give a good opportunity to decrease the DOC which are calculate has $\frac{\$}{km \cdot seat}$ and make aircraft competitiveness on market.

5.4 Flight Deck and pilot visibility

Taking into account the dimensions of the cockpit of the others military aircraft at which we have looked as reference, the *flight deck* has been design to be $3,32\,m$. This dimension guarantee for the flight deck to be fitted with dual controls for the pilot and co-pilot and innovative modern systems like multifunctional displays which are always more powerful and compact as shown in cockpit (fig.5.2).

Figura 5.2: The innovative flight deck of the Xian MA-700

It is important to note that the XIAN MA-700 is a civil aircraft and that the system in its cockpit are lesser than those which a military aircraft need. For these reasons, for our purpose, we have adopted the CASA C-295M cockpit as case example.

To guarantee the best visibility to the pilot, the minimum angle are:

- 10° under the horizon line during climbing;
- 20° over the horizon line during turn;
- 110° sideways during turn.

The chosen angle are shown in Fig.5.3.

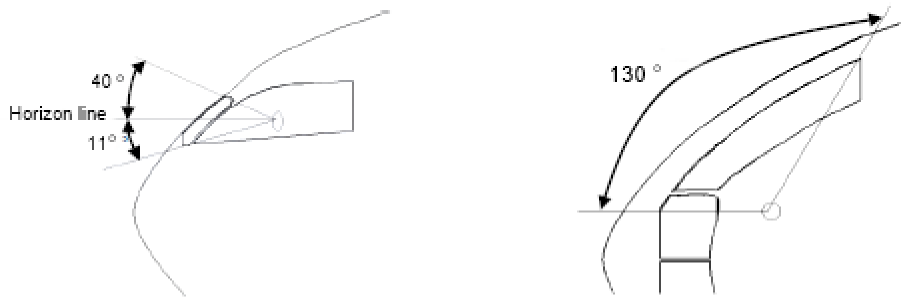

Figura 5.3: Pilot visibility angles

5.5 Tail cone angle

Considering similar aircraft it has been chosen an upsweet angle of 15° that will allow the right rotation in take-off phase.

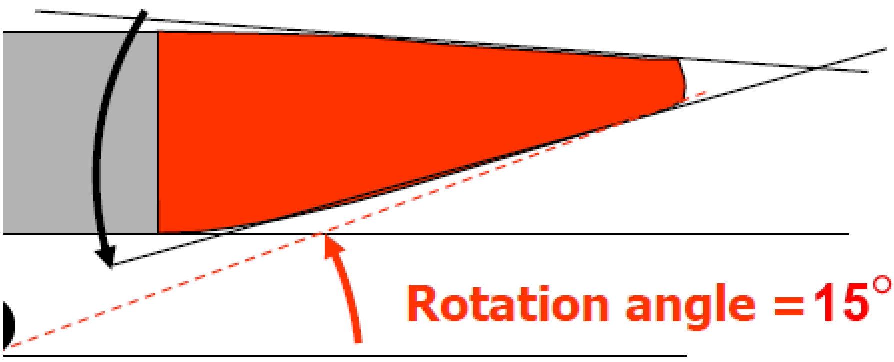

Figura 5.4: Tail cone angle

5.6 Nose and Tail fitness Ratio

The relationship between the length of the nose (or the tail cone) and the maximum external diameter is very important when an aircraft is projected. In fact we need to avoid that the flow is too much accelerated in these zones because it can generates shock waves and separation. In other words we want to avoid wave drags.

Typical value of these relationship are:

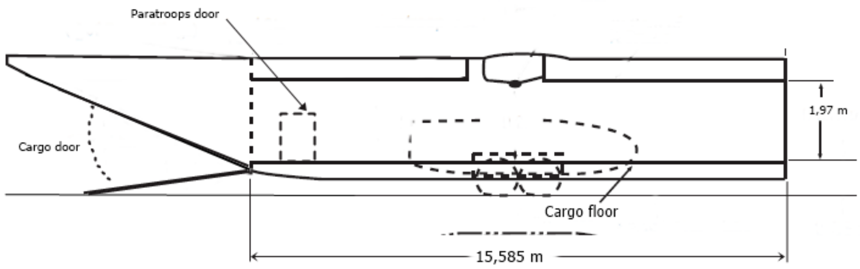

Figura 5.5: Side view of the dimensioned fuselage.

- 1.5 for the nose;
- 1.8-2 for the tail cone.

For our aircraft these values are:

- 1.19 for the nose;
- 2 for the tail cone.

5.7 Dimensioning results

Taking into account the previous paragraphs the fuselage layout are defined as follow:

Tabella 5.2

Cabin length	$15,585\,[m]$
Number of toilettes	1
Toilettes width	$36\,[in]$
Interior diameter	$2,65\,[m]$
External diameter	$2,77\,[m]$
Cabin height	$1,97\,[m]$
Tail cone length	$5,54\,[m]$
Nose length	$3,32\,[m]$
Fuselage length	$\mathbf{28,76}\,[m]$

5.8 Fuselage CAD

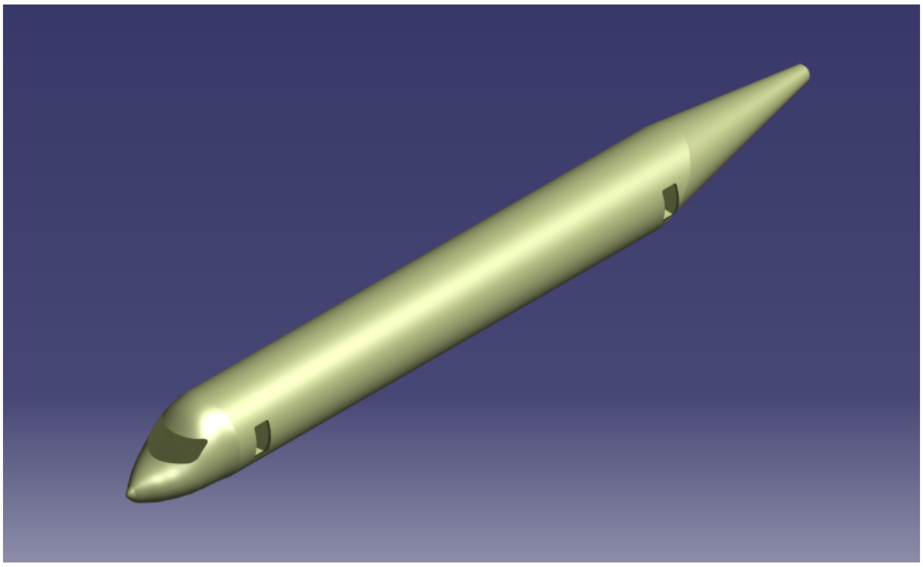

Figura 5.6: CAD of the fuselage layout

Capitolo 6

Propulsion System

6.1 General Characteristics

To be able to chose the suitable propulsion system, first of all it should be known the necessary thrust for the aircraft design. After that, taking into account the required characteristics for the turboprop and that the total number of motors is two, the choice of the most appropriate propulsion systems is reduced to a low number of already developed engines.

This choice has been done considering the economical and technological factors. If the existing engines did not suit the project (after several iterations), then a new propulsion system should be built. Furthermore, it is already known that the vertical location of the wing relative to the fuselage centreline is high. This parameter affects to tail design, landing gear design, and center of gravity among others, but this information is also important for the election of the propulsion system of the air-plane.

For this project, it has been chosen a bi-motor configuration with pylon mounted under the wing. Broadly, this causes the following advantages and disadvantages:

- High asymmetric yaw on engine failure, which requires larger rudder. In conclusion, it means drag penalties.
- Engines provide bending relief on the wing, allowing better wing design (thinner wings), which it means less drag.
- At high incidence angles, the nacelles can prevent span-wise flow: less drag and better stall characteristics.
- Full thrust can impose a large undesirable, pitch up moment, in terms of stall recovery.
- Less freedom in roll on cross-wind landings.

Now it should be observed the factors which compared the probability of engine failure for diverse type of aircraft: Even though the new engines are reliable, it can not be ignored the failure of one of them which will entail to a drastic reduction of thrust and at the same time a huge decrease in roll and yaw moment that turns to an asymmetric conditions of flight. Defining P as the

	Probability of engine failure (per flying hour)		
Failure of	1 engine	2 engines	3 engines
twin-engine aircraft	2P	P^2	-
three-engine aircraft	3P	$3P^2$	P^3
four-engine aircraft	4P	$6P^2$	$4P^3$

Figura 6.1: Engine failure depending on aircraft's configuration

probability of failure, it could be seen that the probability of 1 engine failure for a four-engine aircraft, is twice the probability of a twing-engine aircraft. Among that, we can assume a probability of P^2 for a single-motor failure situation on a twin-engines turboprop (6.1).

Finally, knowing all these parameters and having in mind the turboprop engines used in similar aircraft, the propulsion system elected is Pratt & Whitney PW 150A.

As a first description, the PW 150A is a three spool, free turbine-propeller engine. A three stage axial compressor and a centrifugal compressor are independently driven by a single stage axial turbines, and a two stage axial turbine drives an offset reduction gearbox, as shown in fig. 6.3.

The dimensions and weight of the PW 150A are shown in the following table:

These values were used as an input in the stability programs developed in Matlab.

To sum up the performances for further deeply analysis has been attached the ratings of PW150A:

In future iterations of the project, some surfaces or geometries would be modified in order to achieve the take-off and landing requirements.

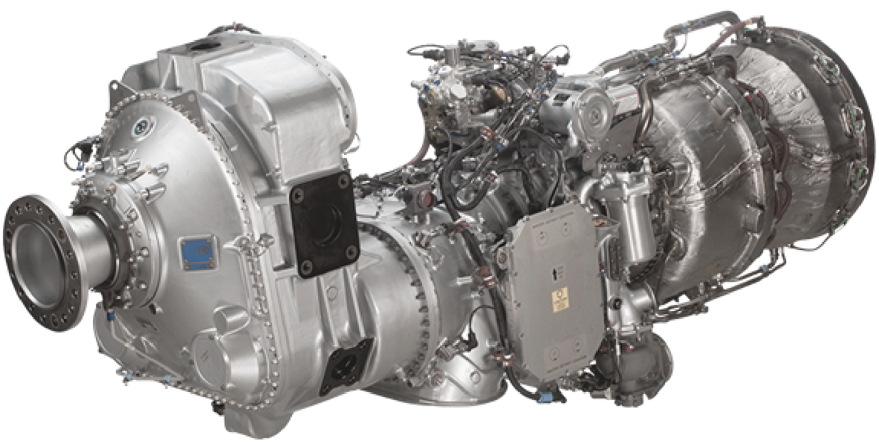

Figura 6.2: Pratt & Whitney PW 150A

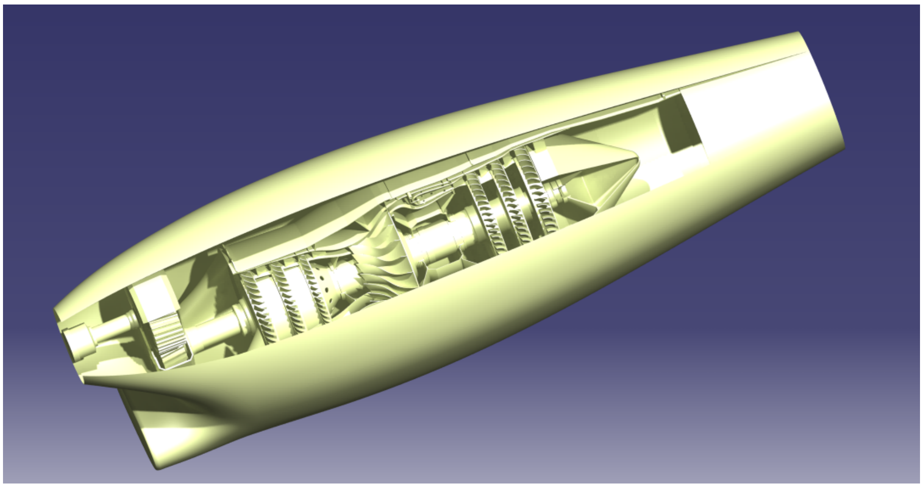

Figura 6.3: CAD of the Pratt & Whitney PW 150A

Engine Model	Overall Length (mm)	Overall Width (mm)	Overall Height (mm)	Dry Spec. Weight (kg)(*)
PW150A	2420	790	1100	716.9

Figura 6.4: Engine dimensions and weight

	Maximum Take-off Power – 5 min.		Normal Take-off Power – 5 min.		Maximum Continuous Power	
Engine Model Ratings at Sea Level	Shaft Power (kW)	Jet Thrust (N)	Shaft Power (kW)	Jet Thrust (N)	Shaft Power (kW)	Jet Thrust (N)
PW150A	3781	3750	3415	3412	3781	3750

Figura 6.5: Engine power ratings

6.2 Propeller Layout

From *"Data collection"* Excel work-sheet, we have obtained two very different types of propeller:

- Hamilton Sundstrand 568F (fig. 6.6);
- Dowty R391 (fig. 6.7).

It is important to note that for our purpose we have to take into account two different aspects choosing the propeller which can best fit our preliminary project:

1. the match with engine;
2. the number of blades.

The first point have been easily solved studying the data sheets and the application those propellers have been developed for.

The Dowty R391 has been introduced for the C-130J in 1996 to match with Rolls-Royce AE 2100 turboprop engine series that can generate a power of 4637 shp[1].
At the same time the Hamilton Sundstrand 568F fitted with the PW-120 turboprop series which can generate about 3000 shp.
Looking at those specifications, as we adopt PW-150A as turboprop for the aircraft we are going to design, we have to chose HS-568F as propeller which best fit our project.

Another reason to chose this propeller can be search looking at the *efficiency* of the propellers.
According to the *Momentum Theory or Disk actuator theory*[2], *efficiency* can be expressed by the term:

$$\eta = \frac{P_a}{P_{engine}} \tag{6.1}$$

[1] [15]
[2] W.J.M. Rankine (1865), A. G. Greenhill (1888) and R.E. Froude (1889)

Figura 6.6: Hamilton Sundstrand 568F

Figura 6.7: Dowty R391

where P_a is the *available power* also know as *propulsive power* which is expressed by:

$$P_a = T \cdot v \tag{6.2}$$

where v is the *velocity* and T is the *thrust*.
At this point we have to take into account some considerations:

- the *Thrust* of a propeller depends on the volume of air accelerated per time unit, on the amount of the acceleration, and on the density of the medium. Based on momentum considerations, it can be expressed by the following formula:

$$T = \frac{\pi}{4} \cdot D^2 \cdot \left(v + \frac{\Delta v}{2}\right) \cdot \rho \cdot \Delta v \tag{6.3}$$

- the definition written in eq.6.1 is not useful for the special case of static thrust. That is simple to demonstrate if we consider that this definition for efficiency contains the velocity v, which means, that the efficiency approaches zero as the flight speed goes to zero, because the thrust cannot become infinitely large. For this reason, neglecting rotational losses (which results in an efficiency loss of 2 to 5 percent for typical propellers), the power absorbed by the propeller can also be expressed by:

$$P_{engine} = T \cdot \left(v + \frac{\Delta v}{2}\right) \tag{6.4}$$

According to those considerations, we can combine the equations above into a relation between the velocity and the efficiency for a given power and diameter:

$$v = \eta \left(\frac{2 \cdot P}{\pi \cdot \rho \cdot D^2(1-\eta)}\right)^{1/3} \tag{6.5}$$

Considering the ideal case in which there is no induced velocity neither friction losses, the equation 6.5 can be plotted as the example in fig.6.8.

Taking into account the purpose of this section, for a propeller working in a certain flow at a certain speed the plot in fig.6.8 can be read as a relation between efficiency, power and diameter. Considering fixed even the engine power, efficiency grow as the diameter decrease. Analysing the two propeller available, the one which has the smaller diameter is the *Hamilton Sundstrand 568F*.

6.2.1 Number of blades

The purpose of this section is not to discuss about the difference between projecting a rotor with 5 blades or 6. It is known that as primary effects, changing the number of blades will modify the *blade solidity* σ which means that for a propeller of certain diameter, to maintain σ constant we had to change the *Mean Aerodynamic chord*. We want to introduce another aspects that should take into account when we made the project of an aircraft for military applications.
Typically, military aircraft have to respond to the requirement of being "invisible" or, at least, not immediately detected by a radar.

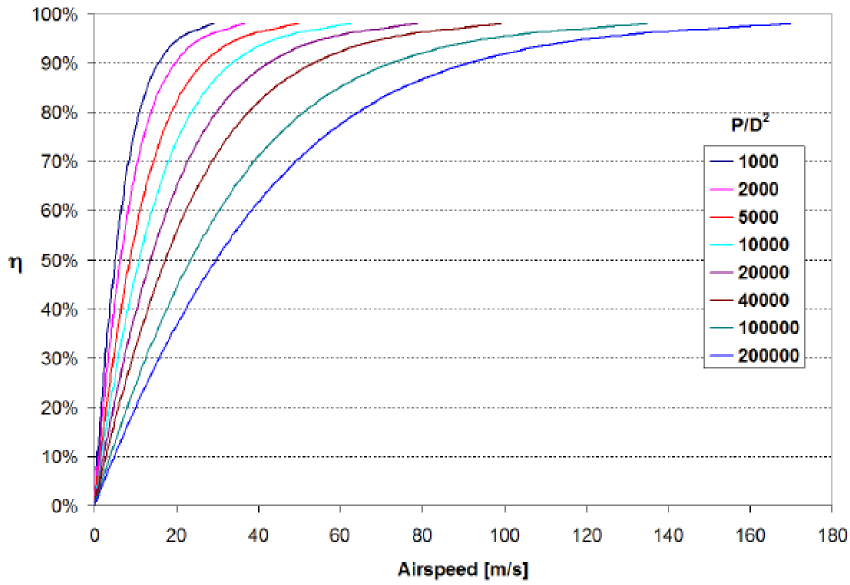

Figura 6.8: Ralation between *airspeed* and *efficiency*

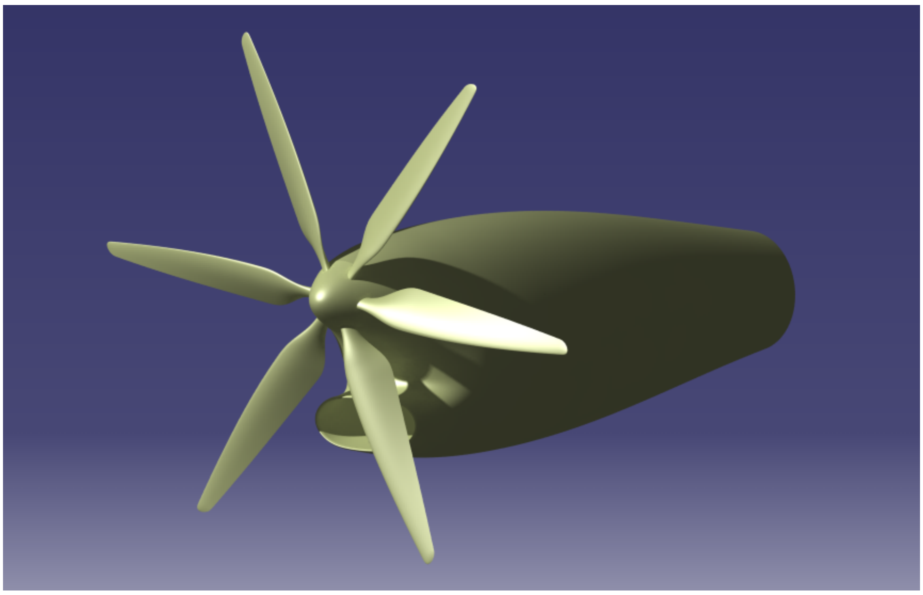

Figura 6.9: CAD of the complete propulsion system.

It is known that the signal reflected by objects in movement face the *doppler effect*, i.e. a translation of the frequency proportional to the velocity. The Doppler shift can be expressed as:

$$\Delta f = \frac{2v}{\lambda} \tag{6.6}$$

where v is the relative velocity between radar and target: positive if the receiver is moving towards the source (and negative in the other direction).

With respect to the blades, the signal suffers a modulation due to the rotation of them. It is important to note that this modulation is unique for each aircraft (that is why they call it *signature*) and it is equivalent to a *flash* on the radar which have detected the target.
The frequency of this *flash* is directly proportional to the number of blades and implementing a simple model propeller rotation we have:

$$F_F = F_R N_b \qquad even\, number\, of\, blades \tag{6.7}$$

$$F_F = 2F_R N_b \qquad uneven\, number\, of\, blades \tag{6.8}$$

According to these considerations, we have chosen an even number of blades which have an halved frequency of flash on the radar detector.

Capitolo 7

Weight estimation

The estimated weight of an aircraft has crucial importance. In fact, a weight reduction typically involves an increase, also important, of costs (for example, you may have to resort to a new technology for the processing of a particular structural element). However, especially for particularly complex aircraft, this is the road less tortuous to reduce operating costs.

The weight of an aircraft, during the phase of preliminary draft is influenced by the choices made with respect to the layout and geometry. Generally, during this stage we analyze various design solutions, while maintaining fixed the performance required in order to assess what configuration offer the best compromise between weight and performance. The estimated weight affects mainly the immediate aftermath to it: the identification of the center of gravity position which, in turn. It has an impact on the determination of the performance until then based on statistical data and/or the result of experience of the designers, and yet to limitations imposed by the regulations.

To evaluate the weight of an aircraft, the aircraft itself may be viewed as a set of components that can be organized into groups, which they can be further separated into components. It therefore seems obvious that, depending on the stage in which you are in, the determination of the weight of the aircraft it can be more and more refined.

At the stage of preliminary design weight estimate is based on methods semi-empirical that, taking as input a limited but significant number of parameters, and by means of an iterative process, estimated with a certain degree of confidence the weight of the aircraft itself. In the following discussion are not commented upon the various terms that appearing in formulas, both for the obviousness of the meaning of some of them, both because they are empirically derived data. The iterative process used is supplied in a MATLAB script attached.

The estimated weights was carried out by two different methods. The first method is presented in the book Synthesis of Subsonic Airplane Design - E. Torenbeek - 1976 - Delft University Press[[12]]; the second in Civil Jet Aircraft Design - L.R. Jenkinson, P. Simpkin, D. Rhodens - 1999 - American Institute of Aeronautics and Astronautics[[13]].

As we shall see, the Torenbeek method is less accurate than Jenkinson's, as the latter also considers the factors that are not present in the first. Here we analyze step by step the procedure followed and the entered parameters.

7.1 Torenbeek's method

The method proposed by Torenbeek evaluates the masses of the various components depending on the weight Maximum take-off (MTOW). The entered coefficients are valid if units from the international system are used.

7.1.1 Structural masses

Wing mass is given by the follow relation:

$$M_W = 0.00667MZFM\left(\frac{b}{\cos\Lambda_{1/2}}\right)^{0.75}\left(1+\left(\frac{1.905\cos\Lambda_{1/2}}{b}\right)\right)n_{ult}^{0.55}\left(\frac{b\cdot t_r/\cos\Lambda_{1/2}}{MZFM/S}\right)$$

The mass of the tail surfaces is estimated by adding the contribution of vertical and horizontal tails.

$$M_T = M_H + M_V$$

$$M_H = K_H S_H\left(0.05386\frac{S_H^0.2V_D}{\sqrt{\cos\Lambda_{1/2}}} - 1.41\right)$$

$$M_V = K_V S_V\left(0.05386\frac{S_V^0.2V_D}{\sqrt{\cos\Lambda_{1/2}}} - 1.41\right)$$

$$K_H = 1.1$$

$$K_v = 1 + 0.15 * S_h * hh/(S_v * bv)$$

$$M_F = K_{land}K_{pres}K_{WF}\sqrt{\frac{V_D L_T}{D_F H_F}}S_F^{1.2}$$

$K_{land} = 1$ for retractile landing gear, $K_{pres} = 1.08$ for pressurized cabin

$$M_{nac} = 0.0065K_{inv}MTOT$$

K_{inv} coefficient taking into account the presence of thrust reversers and MTOT is the thrust [kg].

The weight of the landing gear was measured as the sum of the weights of the nose gear and main landing gear. Both landing gear were retractable considered. The weight of each landing gear is given by the relation

$$\begin{aligned} M_{LG} =& K_{LG}(A_1 + B_1\cdot MTOW^{0.75} + C_1\cdot MTOW^{0.75} + D_1\cdot MTOW^{1.5}) + \\ &+ K_{LG}(A_2 + B_2\cdot MTOW^{0.75} + C_2\cdot MTOW^{0.75} + D_2\cdot MTOW^{1.5}) \end{aligned}$$

where the coefficients A, B, C and D vary according to the type of landing gear used.

Component	**Weight** [kg]
Wing	2331.3
Tail	657.0
Fuselage	1283.7
Landing gear	566.5
Nacelle	644.3
Surface control	371.01

Tabella 7.1: Breakdown structural masses, Torenbeek's method

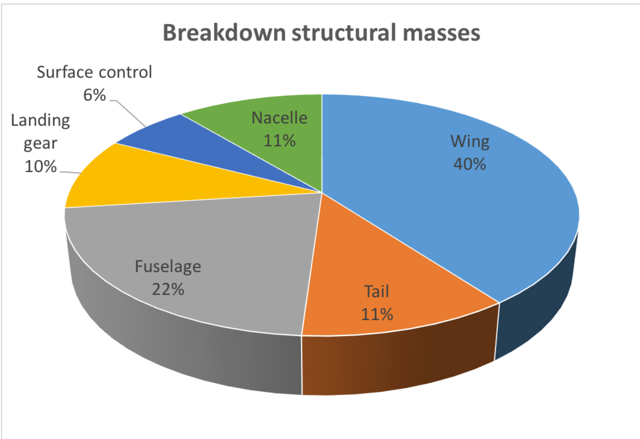

Figura 7.1: Breakdown structural masses, Torenbeek's method

Propulsion system

The weight of the propulsion system was calculated as follow:

$$M_{dry} = 717kg$$

$$M_{powergroup} = 1.35 \cdot (M_{dry} + 0.146 P_{TO})$$

Fuel

From the specifications of engine we have obtained an hourly consumption of about 750 kg/h, and multiplying by the ratio of ESAR and cruising speed we got

$$M_{fuel} = 3900kg$$

Operators

The number of operators has been chosen taking into account the tightest condition in which the aircraft is going to operates. Due to the possibility for this aircraft to load paratroops, a crew of 5 operators (2 pilots + 2 instruments operators + 1 loadmaster operators) has been chosen.

$$M_op = 5 \cdot 95kg$$

Payload

The total payload weight is equal to the sum of the weight of instruments, systems, radar, etc. by which the aircraft will be able to complete missions. It is assumed that the average weight is

$$M_{payload} = 9300kg$$

Facilities and equipment

With facilities and equipment it means the entire grounds of the systems board (such as the APU, the ice protection system and air conditioning, the electric and hydraulic systems etc).

$$M_{FE} = 0.11MTOW$$

Various

The Torenbeek method also considers the masses can not be foreseen with accuracy.

$$M_{various} = 0.01MTOW$$

Component	**Weight** [kg]
Structure	7214.8
Fuel	3900.0
Operators	475
Payload	9300
Power group	1713.2
Equipment	2521.4
Various	229.2

Tabella 7.2: Breakdown masses, Torenbeek's method

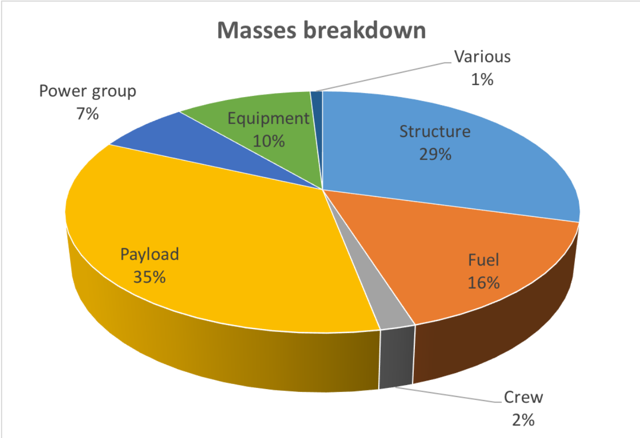

Figura 7.2: Breakdown masses, Torenbeek's method

7.2 Jenkinson's method

Like the Torenbeek's method, Jenkinson method is useful for making a preliminary estimate of the weight of the aircraft. Unlike the Torenbeek's method, Jenkinson method takes into account a state more close to the current one for which the results obtained with this methodologycalculation will be different from the first and the most truthful.

Structural masses

The wing mass is obtainable through the following relation:

$$M_W = 0.021265(MTOW \cdot n_{ult})^{0.4843} S_{ref}^{0.7819} AR_W^{0.993} (1+TR_W)^{0.4} \frac{(1 - R/MTOW)^{0.4}}{\Lambda(t/c)^{0.4}}$$

where

$$R = M_W + M_{fuel} + ((2 * M_{eng} * b_{IE})/(0.4 * b))$$

said Inertia Relief Factor. This factor takes into account the effect of relieving inertial loads on the bending moment on the wing agent. The value obtained, a 5% was deducted because the carts are not positioned in the wing, while it is a 2% was added to the presence of spoilers and airbrakes, for a total of -3% to subtract the value obtained with the formula up.

The mass of the empennage is given by adding the contribution of the vertical and horizontal stabilizers.

$$M_T = M_H + M_V$$

where

$$M_H = S_H K_H$$

$$M_V = S_V K_V$$

Fuselage weight is given by:

$$M_F = 0.039(L_F 2 D_F V_D^{0.5})^{1.5}$$

to which an 8% for pressurization and a 7% is added to the cart in fuselage

Nacelle weight is given by:

$$P_{to} = 3781$$

$$M_nacelle = 0.0852(P_{to})$$

Control surfaces weight is given by:

$$M_{CS} = 0.4 \cdot MTOW^{0.684}$$

Component	**Weight** [kg]
Wing	3315.30
Tail	657.0
Fuselage	1283.7
Nacelles	644.3
Landing gear	618.1
Control surfaces	398.5

Tabella 7.3: Breakdown structural masses, Jenkinson's method

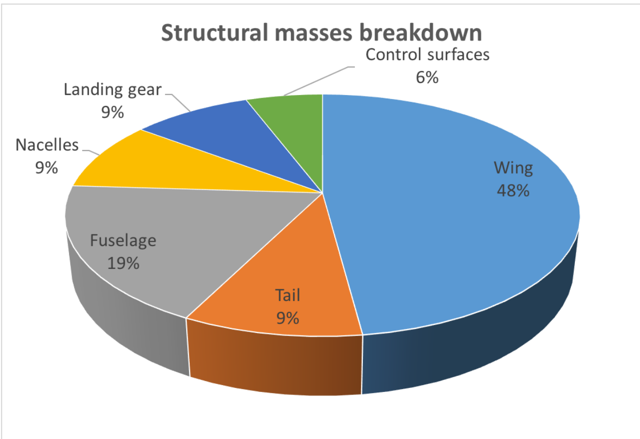

Figura 7.3: Breakdown structural masses, Jenkinson's method

Operators

Crew weight is given by:

$$M_{op} = 93 \cdot 5$$

Propulsion

Propulsion weight is given by:

$$M_{prop} = 1.43 M_E$$

Fuel

Fuel weight is given by:

$$M_fuel = 3900kg$$

Payload

Payload weight is:

$$M_{Payload} = 9300kg$$

Fixed equipment

Fixed equipment weight is given by:

$$M_{FE} = 8\%MOTW + 1\%MTOW$$

Component	**Weight** [kg]
Structure	10238.0
Fuel	3900.0
Operators	465
Payload	9300
Power group	1713.2
Equipment	3133.0

Tabella 7.4: Breakdown masses, Jenkinson's method

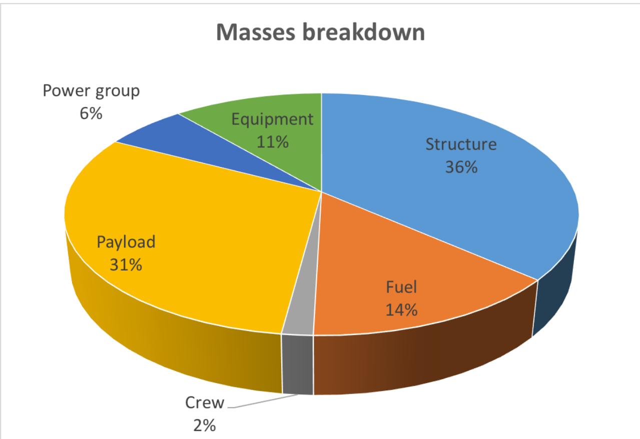

Figura 7.4: Breakdown masses, Jenkinson's method

Capitolo 8

Static Stability

8.1 Airfoil Analysis

In this chapter is analyzed the capacity of the aircraft to response correctly to a perturbation, performing a roll, pitch or yaw moment and put again the airplane in an equilibrium situation. It will be calculated the barycentre's position, the neutral point position, always considering the surface influence (being the fuselage and the generation-lift surfaces). Besides it will be determined the $C_L - \alpha$ and $C_m - \alpha$ curves . To be able to perform this study is essential to have the data from: the aerodynamic study, weight estimation and the geometrical characteristics obtained in the preliminary design. All the study has been performed in the Matlab code 'static_stability.m'.

8.1.1 Barycentre position

From this preliminary design it has been possible to obtain the component's barycentre using the matrix (8.1):

To be able to obtain a acceptable result, it was necessary to make few iterations. It is also know that the turboprop is symmetrical in the plane XZ, so the barycentre will be in this plane. The position of the barycentre comes as a % of the Main Aerodynamic Chord (MAC) and it is indicated with 'h':

$$h = 0.520[m] \tag{8.1}$$

The wing's centre of gravity coincides with the neutral point of the isolated wing, and constitutes the initial point to calculate the neutral point of the complete aircraft:

$$h = 0.25[m] \tag{8.2}$$

Due to the existence of the fuselage (Δh_n), and other elements, the aircraft's gravity centre change his position. To analyse this contribution the diagram in fig.8.2 has been taken into account: Fuselage:

$$\Delta h_{fuselage} = -0.0852 \tag{8.3}$$

Nacelle:

$$\Delta h_{nacelle} = -0.0332 \tag{8.4}$$

```
position_matrix =[M_w/2       17.5        4.25        3;
                  M_w/2       17.5        -4.25       3;
                  M_h/2       29.5        2.28        5;
                  M_h/2       29.5        -2.28       5;
                  M_v         32          0           8.75;
                  M_fus       17.65       0           3.75;
                  M_nac/2     15.61       4.5         1.5;
                  M_nac/2     15.61       -4.5        1.5;
                  M_pg/2      16          4.5         1.5;
                  M_pg/2      16          -4.5        1.5;
                  M_car/2     19          1.25        1;
                  M_car/2     19          -1.25       1;
                  M_fue/4     16.5        3           3;
                  M_fue/4     16.5        -3          3;
                  M_fue/4     18.5        8           3;
                  M_fue/4     18.5        -8          3;
                  M_pay       17.65       0           3.75;
                  M_crew      17.65       0           3.75;
                  M_imp       17.65       0           3.75;
                  M_liq       17.65       0           3.75 ];
```

Figura 8.1: Data input of the barycentre's calculation

Final value of δh_n:

$$\Delta h_{total} = \Delta h_{fus} + 2 \cdot \Delta h_{nacelle} = 0.0985 \tag{8.5}$$

And finally, for the group of wing + fuselage:

$$\Delta h_{nw} = 2.5 \tag{8.6}$$

8.1.2 Neutral point position and Static Margin

The neutral point is obtained as:

$$h_n = h_{nw} + V_H \frac{a_t}{C_L \alpha} = 1.7122 \tag{8.7}$$

The static margin is defined as the margin which the barycentre is allowed to have because the aircraft maintains the safety:

$$h - h_n = -1.1913 \tag{8.8}$$

The value of the margin should be negative to have an acceptable static stability.

8.1.3 Characteristic curves

The $C_m - \alpha$ curve verifies the effects of the static stability on the longitudinal plane when the three statements are true:

- $C_{m0} > 0$ to assure the equilibrium.

- $C_{m\ \alpha} < 0$ to assure the static stability.
- $h < h_n$ to assure that the barycentre is located before of the neutral point

Then the calculations should be made:

$$C_{m0} = C_{m0wb} - V_H a_t (i_t - \epsilon_0) \left[1 - \frac{a_t S_t}{C_L \alpha S} \left(1 - \frac{\partial \epsilon}{\partial \alpha} \right) \right] = 0.2352 \tag{8.9}$$

$$C_m \alpha = C_L \alpha (h - h_n) = -6.1469 \tag{8.10}$$

$$C_m = C_m 0 + C_m \alpha \tag{8.11}$$

When $C_m = 0$ is the equilibrium condition. If it is tried to coincide this condition with the aircraft incidence and using this manner it would not need the trim during the cruise it is necessary to localize in the right position the horizontal stabilizer. This means a change in the values of the aerodynamic design and for this reason it has been iterated a few times to be allowed to obtain the desirable performances of the aircraft.

The $C_L - \alpha$ curve is modified from the previous one because of the fuselage and the stabilizers, which vary the lift angle coefficient. The first $C_{L\alpha}$ obtained was:

$$C_L \alpha = 5.1600 \tag{8.12}$$

$$F = \frac{a_t \cdot S_t}{a_{wb} \cdot S} \left(1 - \frac{\partial \epsilon}{\partial \alpha} \right) = 0.2708 \tag{8.13}$$

And finally:

$$(C_{L\alpha})_{total} = 6.5576 \tag{8.14}$$

The last two plots compare the two curves of $C_L - \alpha$:

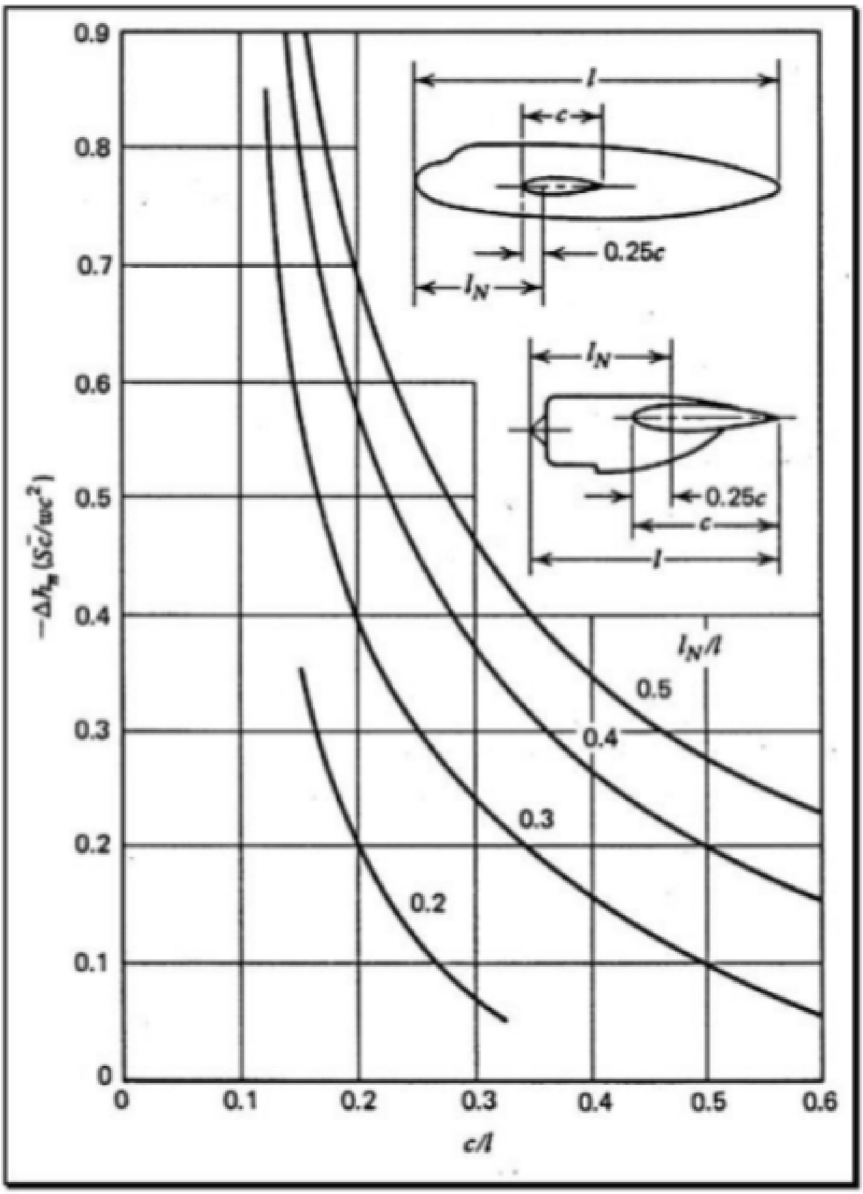

Figura 8.2: Diagram to analyse the contribution of the fuselage.

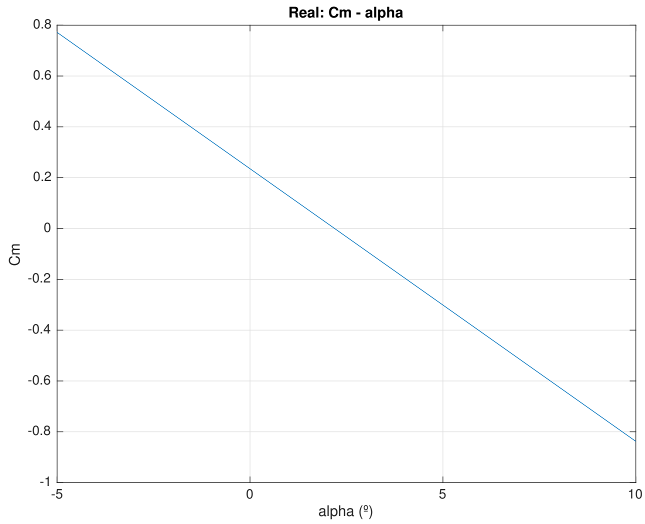

Figura 8.3: Curve $C_m - \alpha$

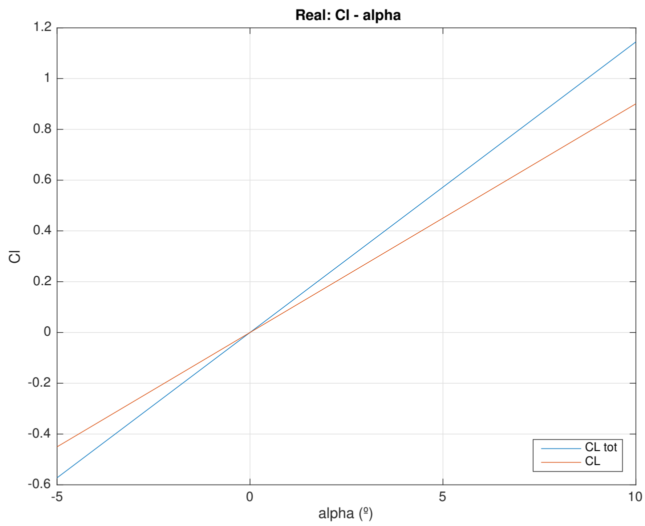

Figura 8.4: Curve $C_L - \alpha$

Capitolo 9

Flight Envelope

During is operation life, an aircraft goes on various load configurations, which depend on flight conditions. To study each of these load configurations, manoeuvre envelope and gust envelope are drawn. The first one is a relationship between load and flight speed and determinates the structural limits which are represented by load factor, and the aerodynamic limits which are represented by the stall curve. The second one factor take into account external forces like gust which induces extra loads on the aircraft.

To study these diagrams has been made reference to the JAR 25.

9.1 Manoeuvre Diagram

First of all we need to calculate the load factors which delimit the diagram. Starting form the maximum load factor, according to the normative, we can calculate it by the equation:

$$n_{MAX} = 2.1 + \frac{24000}{W_{lb} + 10000} = 2.2 \tag{9.1}$$

where W_{lb} is the aircraft weight in pounds. The value we obtain is less than the minimum factor intended by the normative, which impose, for a civil aircraft:

$$2.5 \leq n_{MAX} \leq 3.8 \tag{9.2}$$

So we assume the value:

$$n_{MAX} = 2.5 \tag{9.3}$$

The same normative also impose limits on the minimum load factor. So we assume:

$$n_{min} = -1 \tag{9.4}$$

Once upper and lower limits of the manoeuvre diagram are defined, we can calculate the stall speed, that is the minimum speed which is possible to make the manoeuvre for load factor limits:

$$V_{st}^{+} = \sqrt{\frac{2\left(\frac{W}{S}\right)n_{MAX}}{\rho C_{L\,MAX}^{+}}} = 74.17\,m/s \tag{9.5}$$

$$V_{st}^{-} = \sqrt{\frac{2\left(\frac{W}{S}\right)n_{min}}{\rho C_{L\,min}^{-}}} = 104.90\,m/s \tag{9.6}$$

Where:

- the value of $C_{L\,MAX}^{+}$ and $C_{L\,min}^{-}$ are been calculate in the aerodynamic part;
- the value of air density is the same at see level because we are in a preliminary phase of project so we decide to study the manoeuvre just in this condition even if we know that we should needs to question the air density related to the altitude.

Now we can calculate the next two characteristic points of this diagram:

- $\mathbf{V_A}$, that is the speed below which the aircraft stall before it reach the maximum load factor. It is the intersection between the parabola $n - V$ and the curve at n_{MAX} and should not be less than $V_{st}\sqrt{n_{MAX}}$

$$V_A = 117.28\,m/s \tag{9.7}$$

- the maximum speed in the diagram has been calculated, follow the normative, by:

$$V_D = 1.25 V_C = 250\,m/s \tag{9.8}$$

where V_C is the cruise speed, $V_C = 200\,m/s$.

In Fig.9.1 has been featured the manoeuvre diagram implemented in Excel.

9.2 Gust Diagram

The gust diagram, as we already said, takes into account the variance of the load factor from that one we assume, caused by fluctuation on the atmospheric conditions, i.e. gusts, upward or downward, which instantaneously affect the value of the angle of attack (increase or decrease).

According to the normative:

- gust should be studied as upward gust or downward gust;
- no manoeuvre allowed;
- ignore the pitching moment;
- assume the aircraft as rigid body;

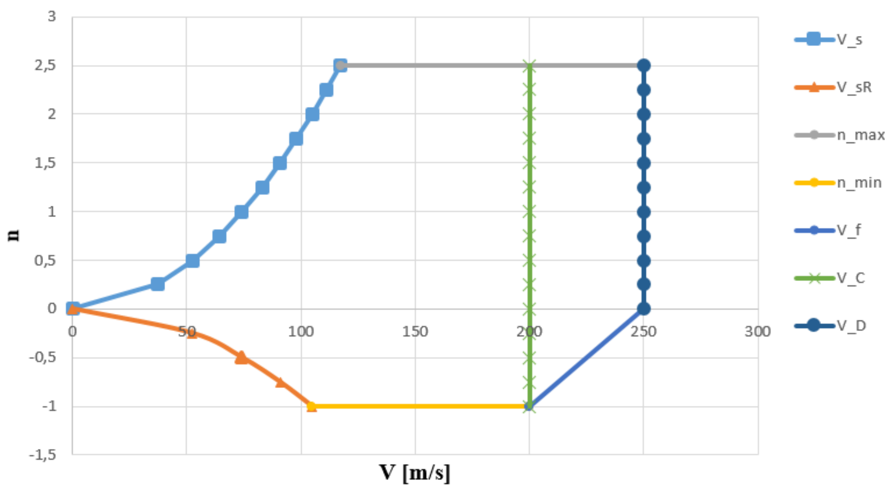

Figura 9.1: Manoeuvre Envelope

- instantaneous aerodynamic changes.

Changes of the load factor are induced by upward gust that is determined through:

$$\Delta n = 1 \pm \frac{K_g U_g V C_{L\alpha}}{\frac{2W}{S}} \tag{9.9}$$

where:

- $\pm$ identify the upward gust $(+)$ and the downward gust $(-)$;
- U_g is the gust velocity in m/s;
- V is the air speed in m/s;
- $K_g = \dfrac{0.88\mu_g}{5.3 + \mu_g}$ is a coefficient that takes into account the dynamic of the aircraft;
- $\mu_g = \dfrac{2\frac{W}{S}}{\rho c g C_{l\alpha}}$ is the aircraft mass ratio;
- c is the geometric mean chord;
- g is the acceleration of gravity.

According to JAR 25,a GA aircraft must be able to withstand gust with a velocity of:

$$0 \leq z \leq 20\,kft \quad \Rightarrow \quad \begin{cases} 66\,ft/s & \text{in corrispondenza di } V_A \\ 50\,ft/s & \text{in corrispondenza di } V_C \\ 25\,ft/s & \text{in corrispondenza di } V_D \end{cases} \tag{9.10}$$

$$z \geq 50\,kft \quad \Rightarrow \quad \begin{cases} 38\,ft/s & \text{in corrispondenza di } V_A \\ 25\,ft/s & \text{in corrispondenza di } V_C \\ 12.5\,ft/s & \text{in corrispondenza di } V_D \end{cases} \tag{9.11}$$

For intermediate altitude, JAR stipulates linear regression to derivate the velocity of gust. So:

$$z = 26.83\,kft \quad \Rightarrow \quad \begin{cases} 59.61\,ft/s & \text{in corrispondenza di } V_A \\ 44.30\,ft/s & \text{in corrispondenza di } V_C \\ 22.15\,ft/s & \text{in corrispondenza di } V_D \end{cases} \tag{9.12}$$

That is, in S.I.:

$$z = 8.179\,km \quad \Rightarrow \quad \begin{cases} 18.17\,m/s & \text{in corrispondenza di } V_A \\ 13.50\,m/s & \text{in corrispondenza di } V_C \\ 6.75\,m/s & \text{in corrispondenza di } V_D \end{cases} \tag{9.13}$$

According to these values of U_g it is possible to feature the following gust diagram (Fig.9.2. The final $V - n$ diagram is featured by the combination of the manoeuvre diagram and the gust diagram (Fig.9.3).

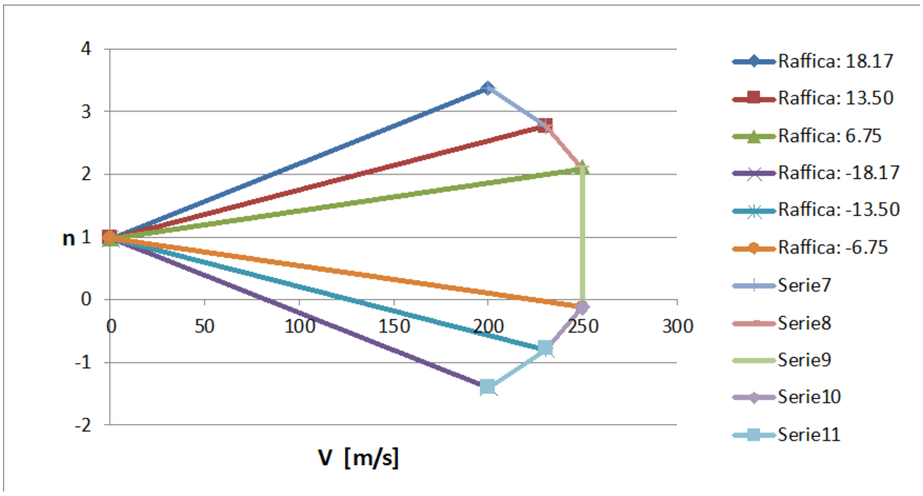

Figura 9.2: Gust Envelope

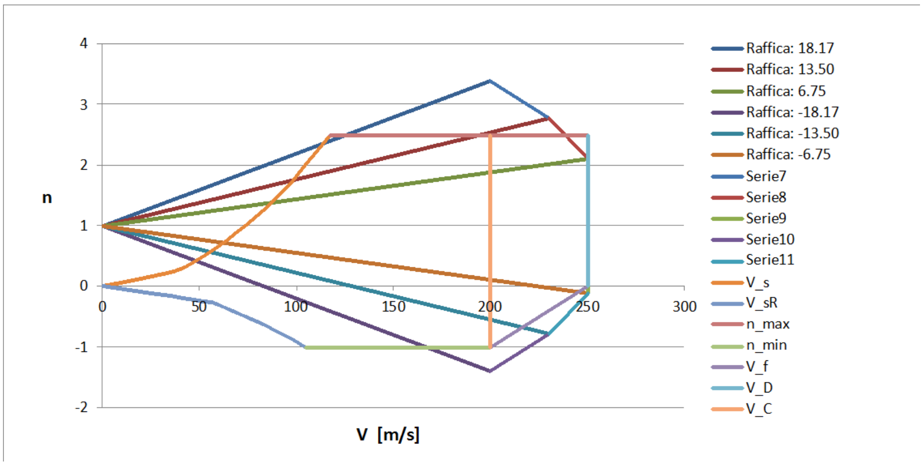

Figura 9.3: $V - n$ Diagram

Capitolo 10

Structural analysis

In this section it is presented the structural analysis made to dimensioning the wing box.
Such analysis have been made for the left wing but, as the wing is symmetric refer to x axis, the results are obviously count towards the right wing.
Starting the analysis, we have to take into account two main points:

1. Determination of loads acting on the wing;
2. Sizing of the wing box.

10.1 Determination of loads acting on the wing

The loads considered in this structural analysis are those that in the cruise phase are more relevant, that is:

1. Aerodynamic loads (lift L and D drag);
2. Total weight of the wing, including the weight of the structural parts (ribs, currents, panels) and other elements that are inside the wing, but who do not have structural tasks (tanks, high lift systems and command and control , fuel pumps, etc.);
3. Fuel Weight;
4. Motor weight.

We will consider the loads applied statically, assuming that the aircraft have no fast dynamics during the cruise phase; the aerodynamic loads, the weight of the wing panel and the weight of the fuel will be treated as distributed loads, while the weight of the engine will be considered a concentrated load.

10.1.1 Statement

The legislation we have referred is the *"CS 25 Large Airplanes"*. The maximum loads expected may act on the aircraft during its operational life are contingency loads (*limit loads*): the structure will have to be able to endure in the elastic range, without permanent deformation, thus the state of stress will not have to exceed the elastic limit (yield) of the material. Furthermore, the temporary deformations must be such as to not affect the ability of the aircraft maneuver. In fact, due to several factors such as:

1. difficult to predict the loads due to the pilot's behaviour and weather conditions;
2. errors in the estimation of the aerodynamic forces;
3. approximations in structural analysis;
4. variations of materials physical property, also due to corrosion phenomena;
5. inaccuracies in the machining of parts and maintenance;
6. deterioration of structural mechanical properties and strength during the exercise (fatigue);

The structure must be designed to withstand the loads of robustness: the contingency loads are multiplied by the appropriate factor of safety (*Safety Factor, SF*) which is typically 1.5. The structure must withstand these loads without breaking for at least 3 seconds and without collapsing, even if they are admitted for permanent deformation. To better quantify the loads acting on the aircraft introduces the load factor n, the ratio between the vertical aerodynamic force and the weight of the aircraft (eq. 10.1). Assuming that the angle of attack is small, you have:

$$n = \frac{L}{W} \tag{10.1}$$

Such n indicates the vertical acceleration in g units to where the aircraft is subjected for a given manoeuvre. From the envelope diagram we can obtain n for the aircraft we are going to design:

1. n_{max} = 2.5;
2. n_{min} = -1.

Whereby, to determine the loads of robustness, we have implemented the equation below (eq. 10.2):

$$robustness\, Load = SF * n_{max} * Load \tag{10.2}$$

where *Load* is the estimated load in the design phase based on the data available from:

- the aerodynamic data;
- the weight estimation of wing, fuel and engine.

10.1.2 Determination of the aerodynamic loads

The aerodynamic loads are considered agents in the direction of the body axis x and z.
The distribution of lift loads along the wing robustness evaluated, is obtained as follows:

$$L = SF \cdot n_{max} \cdot W = n_{ult} \cdot W = 3.75 \cdot W \tag{10.3}$$

$$K_{corr} \cdot A_1 = n_{ult} \cdot W \tag{10.4}$$

where:

$$A_1 = \int_{-b/2}^{b/2} c\, c_l\, dy \tag{10.5}$$

$$n_{ult}\, W = L = \int_{-b/2}^{b/2} \frac{dL}{dy}\, dy \tag{10.6}$$

so we obtain:

$$K_{corr} \int_{-b/2}^{b/2} c\, c_l\, dy = \int_{-b/2}^{b/2} \frac{dL}{dy}\, dy \tag{10.7}$$

and by (eq. 10.7

$$\frac{dL}{dy} = K_{corr}\, c\, c_l \tag{10.8}$$

The last equation (eq. 10.8) that provides the load bearing capacity in strength per length unit along the wingspan.

To estimate the distribution of the resistance loads along the wing we have to:

1. calculate aerodynamic efficiency *E(y)* section by section;
2. get the load distribution of drag section by section *dD/dy* by the equation (eq. 10.9:

$$\frac{dD}{dy} = \frac{1}{E(y)} \frac{dL}{dy} \tag{10.9}$$

It is important to note that the grid used in aerodynamic analysis is denser towards the wing ends, while for structural analysis is more reasonable to use an evenly spaced grid along the half-opening. The distributions of $c\, c_l$ is already available defined with aerodynamic efficiency and grid, to get similar on equally spaced grid *(structural grid)* it will proceed with a simple interpolation, so that on both grids we can have the same distribution. The structural grid is modified so as to have 20 sections of calculation, namely to have ribs 20 along the half-opening, approximately one each meter. Once we have obtained the loads distributed *dL/dy* and *dD/dy*, we have to transfer them from the wind axes to body axes. It is considered positive:

- down-force along the body axis z ($q_{z\,aer}$) if directed from the belly to the back of the pros;
- down-force along the body axis x ($q_{x\,aer}$) if directed from the leading edge to the trailing edge.

With these agreements, we can write:

$$q_{x\,aer} = \frac{dD}{dy} \cos\alpha' - \frac{dL}{dy} \sin\alpha' \tag{10.10}$$

$$q_{z\,aer} = \frac{dL}{dy} \cos\alpha' + \frac{dD}{dy} \sin\alpha' \tag{10.11}$$

where α is the angle of the wing fitting (α_{fly} spreadsheet aerodynamics).

Section	aerodynamic y [m]	structural [m]	aerodynamic chord [m]	structural chord [m]	ccl aero [m]	ccl struct [m]
1	0.0000	0.000	2.54	2.54	2.3883	2.386831399
2	0.7083	0.711	2.54	2.54	2.3852	2.38749
3	1.4167	1.421	2.54	2.54	2.3754	2.377878005
4	2.1250	2.132	2.54	2.54	2.3569	2.354866718
5	2.8333	2.842	2.54	2.54	2.3224	2.317662265
6	3.5417	3.553	2.4647	2.464666667	2.2673	2.267057012
7	4.2500	4.263	2.3893	2.389333333	2.2021	2.204768847
8	4.9584	4.974	2.314	2.314	2.1301	2.132868341
9	5.6667	5.684	2.2387	2.238666667	2.052	2.053293773
10	6.3750	6.395	2.1633	2.163333333	1.9681	1.967454023
11	7.0834	7.105	2.088	2.088	1.8777	1.875919343
12	7.7917	7.816	2.0127	2.012666667	1.7801	1.778199982
13	8.5000	8.526	1.9373	1.937333333	1.6735	1.672612698
14	9.2084	9.237	1.862	1.862	1.5557	1.556235129
15	9.9167	9.947	1.7867	1.786666667	1.4235	1.424948032
16	10.6251	10.658	1.7113	1.711333333	1.2722	1.273565397
17	11.3334	11.368	1.636	1.636	1.0958	1.096052433
18	12.0417	12.079	1.5607	1.560666667	0.887	0.885831411
19	12.7501	12.789	1.4853	1.485333333	0.6372	0.636175389
20	13.4584	13.500	1.41	1.41	0.3399	0.340689802

Tabella 10.1: Comparison between aerodynamic and structural grid

10.1.3 Determination of the loads due to the weight of the wing, fuel and engine

To calculate the distribution of load due to the weight of the wing it has been followed the procedure below:

1. we start from the wing overall mass, obtained in the relative weight estimation section;
2. the overall load of robustness is:
$$P_R = n_{ult}\, g\, m_{wing} \tag{10.12}$$
3. distributing the load of strength on the net wing area plan, we have obtained the pressure (eq. 10.13:
$$p_{wing\,weight} = \frac{P_R}{S_{net}} = \frac{n_{ult}\, g\, m_{wing}}{S_{net}} \tag{10.13}$$
4. for each section, we have obtained the load per unit of length of the wing due to the weight multiplying $p_{wing\,weight}$ for the local chord (eq. 10.14):
$$n_{ult}\frac{dW_{wing}}{dy} = -\frac{n_{ult} g\, m_{wing}\, c(y)}{S_{net}} \tag{10.14}$$
where the minus sign due to the fact that the loads downward are considered negative.

With regards to the load due to the fuel weight, we have followed the same previous steps:

1. we start from the fuel mass contained in the wing;
2. the overall robustness load is:
$$P_R = n_{ult}\, g\, m_{fuel} \tag{10.15}$$
3. distributing the load on the surface of the wing part of the plant occupied by the tanks, we have got the pressure (eq. 10.16:
$$p_{fuel} = \frac{P_R}{S_{tanks}} = \frac{n_{ult}\, g\, m_{fuel}}{S_{tanks}} \tag{10.16}$$
4. for each section that falls inside the tanks, we obtain the load per unit length due to the fuel weight by multiplying p_{fuel} for the local chord:
$$n_{ult}\frac{dW_t}{dy} = -\frac{n_{ult}\ g\ m_{fuel}\ c(y)}{S_{tanks}} \tag{10.17}$$

Finally, the robustness load due to the engine weight is:

$$P_R = -n_{ult}\, g\, m_{prop} = -3.751 \cdot 9.81 \cdot m_{prop} \tag{10.18}$$

The total distribution of load along z "q_z" has been calculated by summing the previous contributions of q_{zaer}, the load distributed due to the weight of the wing panel and the distributed load due to the fuel:

$$q_z = q_{z\,aer} + n_{ult}\frac{dW_w}{dy} + n_{ult}\frac{dW_t}{dy} \tag{10.19}$$

10.1.4 Calculation of stress characteristics

Once set loads, we proceed with the calculation of the stress characteristics and the shear and moment diagrams on the wing panel.
The shear T_x and T_z are obtained by integrating respectively q_x q_z, while the moments M_x (moment around the longitudinal axis x) and M_z (moment around the vertical axis z) are obtained, respectively, from the integration of T_z and T_x. Figures 10.1 and 10.2 show the numerical diagrams of interest.

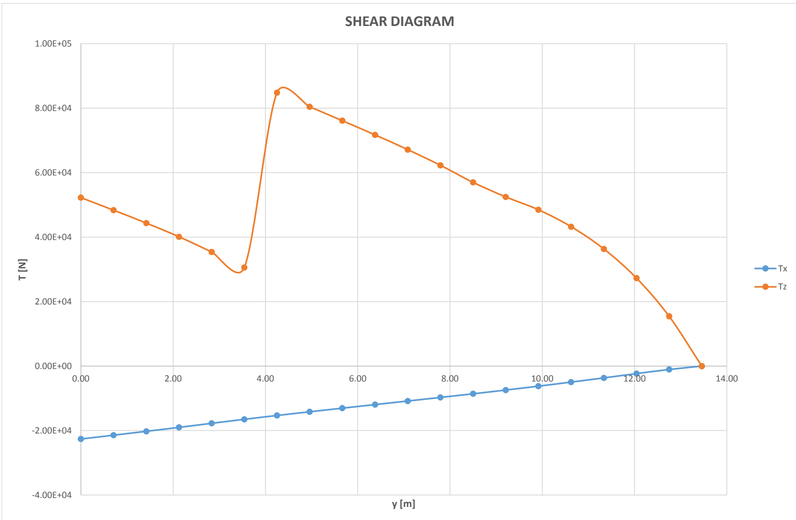

Figura 10.1: Shear diagram

Section	Structural y [mm]	Chord [mm]	ccl (structural) [m]	dL/dy dL/dy [N/mm]	Wing load n*dWa/dy [N/mm]	Fuel load n*dWs / dy [N/mm]	ccd [m]	dD/dy [N/mm]	qz [N/mm]	qx [N/mm]
1	0.0000	2540.0000	2.3868	59.69	-59.68	-5.45	0.0668	1.67	5.44	-1.67
2	710.5263	2540.0000	2.3875	59.61	-59.68	-5.45	0.0670	1.68	5.52	-1.68
3	1421.0526	2540.0000	2.3779	59.37	-59.68	-5.45	0.0680	1.70	5.76	-1.70
4	2131.5789	2540.0000	2.3549	58.91	-59.68	-5.45	0.0701	1.75	6.23	-1.75
5	2842.1053	2540.0000	2.3177	58.04	-59.68	-5.45	0.0721	1.80	7.09	-1.80
6	3552.6316	2464.7000	2.2671	56.67	-57.91	-5.29	0.0682	1.71	6.54	-1.71
7	4263.1579	2389.3000	2.2048	55.04	-56.14	-5.13	0.0659	1.65	6.23	-1.65
8	4973.6842	2314.0000	2.1329	53.24	-54.37	-4.97	0.0638	1.60	6.10	-1.60
9	5684.2105	2238.7000	2.0533	51.29	-52.60	-4.81	0.0629	1.57	6.12	-1.57
10	6394.7368	2163.3000	1.9675	49.19	-50.83	-4.64	0.0623	1.56	6.28	-1.56
11	7105.2632	2088.0000	1.8759	46.93	-49.06	-4.48	0.0624	1.56	6.61	-1.56
12	7815.7895	2012.7000	1.7782	44.49	-47.29	-4.32	0.0631	1.58	7.12	-1.58
13	8526.3158	1937.3000	1.6726	41.83	-45.52	-4.16	0.0647	1.62	7.85	-1.62
14	9236.8421	1862.0000	1.5562	38.88	-43.75	0.0000	0.0666	1.67	4.87	-1.67
15	9947.3684	1786.7000	1.4249	35.58	-41.98	0.0000	0.0695	1.74	6.40	-1.74
16	10657.8947	1711.3000	1.2736	31.80	-40.21	0.0000	0.0725	1.81	8.41	-1.81
17	11368.4211	1636.0000	1.0961	27.39	-38.44	0.0000	0.0750	1.88	11.05	-1.88
18	12078.9474	1560.7000	0.8858	22.17	-36.67	0.0000	0.0750	1.88	14.50	-1.88
19	12789.4737	1485.3000	0.6362	15.93	-34.90	0.0000	0.0689	1.72	18.97	-1.72
20	13500.0000	1410.0000	0.3407	8.50	-33.13	0.0000	0.0496	1.24	24.63	-1.24

Tabella 10.2: Load contribution

Shear due to qz N	Shear due to qx N	Engine Load N	Tz N	Tx N	Mz Nm	Mx Nm
1.11E+05	-2.26E+04	-5.88E+04	5.22E+04	-2.26E+04	1.53E+08	6.71E+08
1.07E+05	-2.14E+04	-5.88E+04	4.84E+04	-2.14E+04	1.37E+08	6.36E+08
1.03E+05	-2.02E+04	-5.88E+04	4.44E+04	-2.02E+04	1.22E+08	6.03E+08
9.89E+04	-1.90E+04	-5.88E+04	4.01E+04	-1.90E+04	1.08E+08	5.73E+08
9.42E+04	-1.77E+04	-5.88E+04	3.54E+04	-1.77E+04	9.53E+07	5.46E+08
8.93E+04	-1.65E+04	-5.88E+04	3.06E+04	-1.65E+04	8.32E+07	5.23E+08
8.48E+04	-1.53E+04	0.00E+00	8.48E+04	-1.53E+04	7.19E+07	4.82E+08
8.04E+04	-1.42E+04	0.00E+00	8.04E+04	-1.42E+04	6.15E+07	4.23E+08
7.61E+04	-1.30E+04	0.00E+00	7.61E+04	-1.30E+04	5.19E+07	3.68E+08
7.17E+04	-1.19E+04	0.00E+00	7.17E+04	-1.19E+04	4.30E+07	3.16E+08
6.72E+04	-1.08E+04	0.00E+00	6.72E+04	-1.08E+04	3.50E+07	2.66E+08
6.23E+04	-9.72E+03	0.00E+00	6.23E+04	-9.72E+03	2.77E+07	2.21E+08
5.70E+04	-8.59E+03	0.00E+00	5.70E+04	-8.59E+03	2.12E+07	1.78E+08
5.25E+04	-7.42E+03	0.00E+00	5.25E+04	-7.42E+03	1.55E+07	1.40E+08
4.85E+04	-6.22E+03	0.00E+00	4.85E+04	-6.22E+03	1.07E+07	1.04E+08
4.32E+04	-4.96E+03	0.00E+00	4.32E+04	-4.96E+03	6.73E+06	7.13E+07
3.64E+04	-3.65E+03	0.00E+00	3.64E+04	-3.65E+03	3.68E+06	4.32E+07
2.73E+04	-2.32E+03	0.00E+00	2.73E+04	-2.32E+03	1.57E+06	2.06E+07
1.54E+04	-1.05E+03	0.00E+00	1.54E+04	-1.05E+03	3.72E+05	5.47E+06
0.00E+00	0.00E+00	0.00E+00	0.00E+00	0.00E+00	0.00E+00	0.00E+00

Tabella 10.3: Shear and moment values

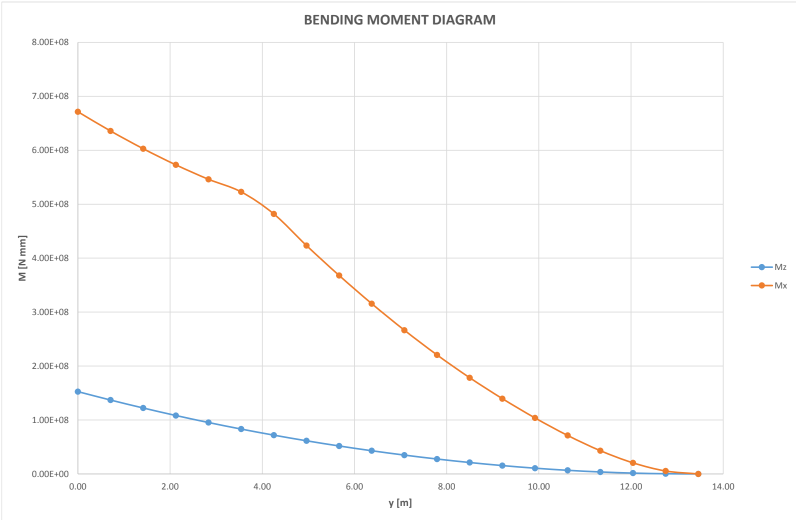

Figura 10.2: Bending moment diagram

10.2 Sizing of the wing box

It is assumed that the wing box is the only structure resistant of the wing, then we proceed with the dimensioning of robustness of the same.

10.2.1 Wing box geometry

The first step has been the adoption of a wing with a double spar: the front and rear spar were fixed to the 15% and 80% of the local chord respectively, across the span. In the plan view of the wing shown in figure below is highlights the arrangement of the longitudinal members.
The wing box is formed by two beams with C section and four panels, two on the top and two on the bottom. Each of the two spars is constituted in turn by a core and two insoles. The length of the root insoles, both front and rear script was fixed at 100 mm. The body shape is defined so that it fits to the profiles arranged along the wing panel.
For each calculation section, the adopted reference system (x,z), has its origin in the leading edge of the local profile. The x-coordinates of points delimiting the caisson, normalized with respect to the local chord c, are:

1. x_1/c = 0.15: x-coordinate of front spar web;
2. x_2/c = 0.15 +((length front spar cap)/c): the length of the cap will follow the same law of taper of the wing tip chord. Therefore in a generic section the length of the spar cap will be given by the product of the length of the root spar cap for the taper local ratio (the ratio of the local chord and the root chord);

3. x_3/c = 0.475: x-coordinate average of the x-axis of the soul front and rear;
4. x_4/c = 0.8 - ((length rear spar cap)/c);
5. x_5/c = 0.8: Rear spar web abscissa.

We have replaced later the non-dimensional values of abscissa in the equations of polynomial interpolation profiles, getting the ordered normalized with respect to the chord. It is obvious that to obtain the values of x and z effective for the section, we have to increase the non-dimensional values for the local chord. By repeating the process for each section we can get the discretization of the structure of the wing box in two spar cap and two panels, both for the back that for the belly, and two cores.

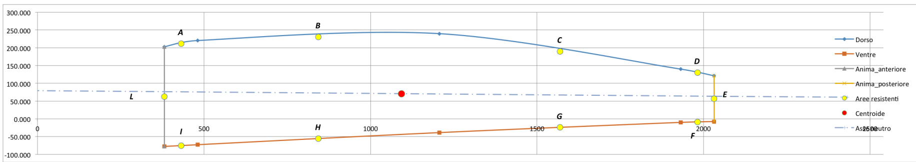

Figura 10.3: Section of the wing box with the various elements used in the calculation

Once the box is discretized, applying the half-shell model: the various structural parts are replaced with equivalents resistant areas, areas concentrated with dimensions equal to those of the corresponding actual structural parts, centred at the respective centres of gravity. The result is shown in figure 10.3.Taking into account the Section 1, resistant areas are designated from letter A to L. In particular:

- A, D, F, I are the resistant areas relating to spar caps;
- B, C, G, H are the resistant areas relating to the panels;
- E, L are the resistant areas related to spar webs.

10.2.2 Stress and strain calculation

First of all we have to calculate the centroid of the resistant areas, defined by the relationships:

$$x_c = \frac{\sum E_i A_i x_i}{\sum E_i A_i} \tag{10.20}$$

$$z_c = \frac{\sum E_i A_i z_i}{\sum E_i A_i} \tag{10.21}$$

Later, we have calculated the moments of inertia of the resistant areas compared to *centroid* of the section, to be included in the Navier formula. For their calculus first we have follow these steps:

1. obtain the central moments of inertia,that is barycentric and main axes X-Z of the resistant area;

Section	y [mm]	Thickness [mm]									
		A	B	C	D	E	I	H	G	F	L
1	0.000	18.00	20.00	18.00	8.00	2.00	2.00	16.00	24.00	20.00	2.00
2	0.708	18.00	20.00	18.00	8.00	2.00	2.00	16.00	22.00	20.00	2.00
3	1.417	18.00	20.00	18.00	8.00	2.00	2.00	16.00	22.00	20.00	2.00
4	2.125	18.00	20.00	18.00	8.00	2.00	2.00	16.00	22.00	20.00	2.00
5	2.833	18.00	18.00	18.00	8.00	2.00	2.00	16.00	22.00	20.00	2.00
6	3.542	18.00	18.00	18.00	8.00	2.00	2.00	16.00	22.00	20.00	2.00
7	4.250	16.00	18.00	16.00	8.00	2.00	2.00	14.00	22.00	20.00	2.00
8	4.958	16.00	16.00	16.00	8.00	2.00	2.00	14.00	22.00	20.00	2.00
9	5.667	16.00	16.00	16.00	8.00	2.00	2.00	14.00	22.00	20.00	2.00
10	6.375	16.00	16.00	16.00	8.00	2.00	2.00	14.00	14.00	16.00	2.00
11	7.083	16.00	16.00	16.00	8.00	2.00	2.00	12.00	14.00	14.00	2.00
12	7.792	16.00	16.00	16.00	8.00	2.00	2.00	12.00	14.00	14.00	2.00
13	8.500	14.00	14.00	14.00	8.00	2.00	2.00	10.00	10.00	10.00	2.00
14	9.208	14.00	14.00	14.00	8.00	2.00	2.00	10.00	10.00	10.00	2.00
15	9.917	14.00	14.00	14.00	8.00	2.00	2.00	10.00	10.00	10.00	2.00
16	10.625	14.00	14.00	14.00	8.00	2.00	2.00	10.00	10.00	10.00	2.00
17	11.333	6.00	6.00	6.00	2.00	2.00	2.00	2.00	6.00	6.00	2.00
18	12.042	2.00	2.00	2.00	2.00	2.00	2.00	2.00	2.00	2.00	2.00
19	12.750	2.00	2.00	2.00	2.00	2.00	2.00	2.00	2.00	2.00	2.00
20	13.458	2.00	2.00	2.00	2.00	2.00	2.00	2.00	2.00	2.00	2.00

2. describe the moments calculated with respect to the axis x^* and z^* calculated in relation to the original resistant area, but parallel to the axes x and z of the section, using the following formulas:

$$J_{x^*} = \frac{J_X + J_Z}{2} + \frac{J_X - J_Z}{2}\cos(2\alpha) - J_{XZ}\sin(2\alpha) \tag{10.22}$$

$$J_{z^*} = \frac{J_X + J_Z}{2} - \frac{J_X - J_Z}{2}\cos(2\alpha) + J_{XZ}\sin(2\alpha) \tag{10.23}$$

$$J_{x^* z^*} = \frac{J_X - J_Z}{2}\sin(2\alpha) + J_{XZ}\cos(2\alpha) \tag{10.24}$$

where α is the rotation angle between the two reference systems, positive if takes X toward Z. The absolute value of this angle represents the inclination of discretized box element compared to x axis.

We can note that the centrifugal moment J_{XZ} is null because axis X and Z of every resistant area are principal axis of inertia. At the end we calculate inertia moments of resistant area regard axis x_c-z_c, with origin on the centroid of the section and parallel to the axis x-z, through the transposition formulas:

$$J_{x_c} = J_{x^*} + A(z - z_c)^2 \tag{10.25}$$

$$J_{z_c} = J_{z^*} + A(x - x_c)^2 \tag{10.26}$$

$$J_{x_c z_c} = J_{x^* z^*} + A(x - x_c)(z - z_c) \tag{10.27}$$

where A is the value of resistant area and x e z are their coordinates regards reference system x-z.

By the Navier's formula it has been possible to obtain the tensions in the resistant areas:

$$\sigma_y = \frac{M_z^*}{J_{z_c}}(x - x_c) + \frac{M_x^*}{J_{x_c}}(z - z_c) \tag{10.28}$$

where:

$$M_x^* = -\frac{M_x + M_z j_z}{1 - j_x j_z} \tag{10.29}$$

$$M_z^* = \frac{M_z + M_x j_x}{1 - j_x j_z} \tag{10.30}$$

$$j_x = \frac{J_{x_c z_c}}{J_{x_c}} \tag{10.31}$$

$$j_z = \frac{J_{x_c z_c}}{J_{z_c}} \tag{10.32}$$

The relative ε_y is given by:

$$\varepsilon_y = \frac{\sigma_y}{E} \tag{10.33}$$

where E is the Young modulus of material.

At this point we have to dimension the thickness's of the various structural elements of the body, section by section, in such a way that the field of resulting tensions does not exceed the values of the ultimate strength of the materials chosen. We have assigned random thickness, and after calculated the corresponding tension range: if the tension is acceptable (no more than ultimate values) then the thickness's are frozen; if not we have reassigned all or some of them, and looping the process until we reached the optimal tension range. In the table **??** it is shown the assigned final thickness's.

In the scheme we have used the spar web areas are very close to the neutral axis and in addiction these structural elements mainly resist to shear. For these two reasons, in resistant areas related to spar web σ_y will be very low.

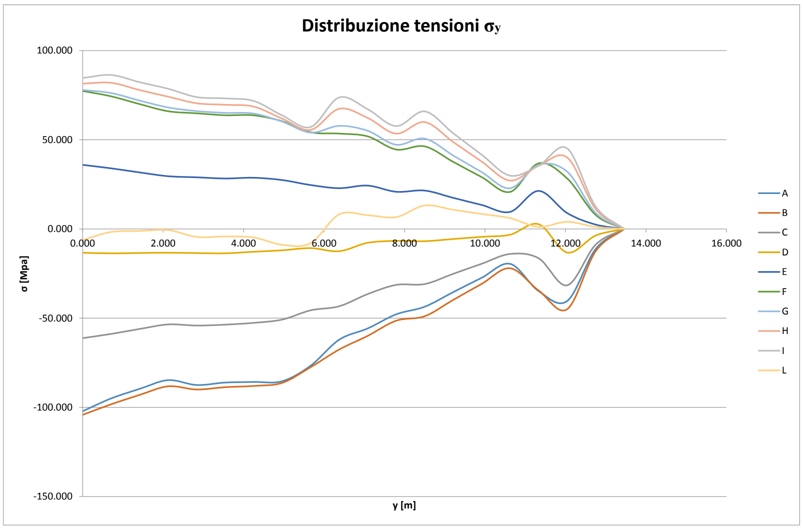

Figura 10.4: Sigma distribution over wingspan for the elements

10.2.3 Deflection calculation

For the calculation of the deflection we have used the principle of virtual work. Consider a state of internal tensions σ_e in equilibrium with the applied loads system. For the same structure will then consider a displacement system η_c, compatible with the constraints imposed on the system, to which is associated the small deformations and congruent system ε_c. PVW states that in equilibrium conditions there is the following equality:

$$L_{ex}^{ec} = L_{int}^{ec} \tag{10.34}$$

Choosing as a system of balanced forces a unitary fictional explorer load (the congruent displacement system is the wing that is being studied, for which we want to precisely determine the deflection), we can get the work that this load will make on the real displacement system and then calculate the deflection:

$$1^e * \eta^c = \int \left(\frac{M_z^{*e}}{J_z} x + \frac{M_x^{*e}}{J_x} z \right) * \left(\frac{M_z^{*c}}{EJ_z} x + \frac{M_x^{*c}}{EJ_x} z \right) dy \tag{10.35}$$

Section	y [mm]	σ_y [MPa]									
		A	B	C	D	E	I	H	G	F	L
1	0.000	-102.160	-104.182	-61.188	-13.329	35.937	77.361	77.929	81.489	84.640	-6.181
2	0.708	-94.991	-98.277	-58.834	-13.666	33.990	74.356	76.191	81.932	86.314	-1.674
3	1.417	-89.646	-93.011	-56.044	-13.460	31.696	70.000	71.982	77.858	82.263	-1.135
4	2.125	-84.749	-88.202	-53.517	-13.302	29.573	66.001	68.131	74.155	78.596	-0.617
5	2.833	-87.473	-89.979	-54.139	-13.520	28.960	64.848	66.076	70.464	73.946	-4.442
6	3.542	-86.097	-88.694	-53.639	-13.641	28.298	63.756	65.086	69.631	73.192	-4.211
7	4.250	-85.760	-87.987	-52.628	-12.772	28.715	63.715	64.700	68.604	71.784	-4.750
8	4.958	-85.338	-86.271	-50.798	-11.958	27.427	60.391	60.185	61.850	63.684	-8.852
9	5.667	-76.624	-77.462	-45.609	-10.734	24.632	54.231	54.046	55.542	57.188	-7.944
10	6.375	-62.075	-67.589	-43.323	-12.457	22.865	53.466	57.801	67.376	73.711	8.183
11	7.083	-55.767	-59.921	-36.508	-7.756	24.318	51.917	55.029	62.248	67.145	7.729
12	7.792	-47.846	-51.424	-31.347	-6.677	20.854	44.547	47.230	53.449	57.665	6.661
13	8.500	-43.588	-48.922	-30.886	-6.856	21.520	46.304	50.660	59.913	65.909	13.175
14	9.208	-35.410	-39.778	-25.153	-5.628	17.455	37.624	41.196	48.773	53.680	10.778
15	9.917	-27.368	-30.780	-19.504	-4.412	13.462	29.086	31.881	37.801	41.630	8.407
16	10.625	-19.565	-22.036	-13.999	-3.207	9.600	20.800	22.828	27.114	29.884	6.077
17	11.333	-34.848	-34.516	-16.435	2.649	21.336	36.804	35.957	35.409	35.503	1.166
18	12.042	-40.371	-44.947	-31.570	-13.200	8.911	28.317	32.117	40.052	45.145	4.010
19	12.750	-11.200	-12.480	-8.779	-3.684	2.458	7.850	8.914	11.133	12.556	1.130
20	13.458	0.000	0.000	0.000	0.000	0.000	0.000	0.000	0.000	0.000	0.000

Tabella 10.4: Stress σ_y

Section	y [mm]	$\mu\varepsilon_y$ [MPa]									
		A	B	C	D	E	I	H	G	F	L
1.00	0.00	-1.40E-03	-1.43E-03	-8.38E-04	4.92E-04	4.92E-04	1.06E-03	1.07E-03	1.12E-03	1.16E-03	-8.47E-05
2.00	0.71	-1.30E-03	-1.35E-03	-8.06E-04	4.66E-04	4.66E-04	1.02E-03	1.04E-03	1.12E-03	1.18E-03	-2.29E-05
3.00	1.42	-1.23E-03	-1.27E-03	-7.68E-04	4.34E-04	4.34E-04	9.59E-04	9.86E-04	1.07E-03	1.13E-03	-1.55E-05
4.00	2.13	-1.16E-03	-1.21E-03	-7.33E-04	4.05E-04	4.05E-04	9.04E-04	9.33E-04	1.02E-03	1.08E-03	-8.45E-06
5.00	2.83	-1.20E-03	-1.23E-03	-7.42E-04	3.97E-04	3.97E-04	8.88E-04	9.05E-04	9.65E-04	1.01E-03	-6.09E-05
6.00	3.54	-1.18E-03	-1.21E-03	-7.35E-04	3.88E-04	3.88E-04	8.73E-04	8.92E-04	9.54E-04	1.00E-03	-5.77E-05
7.00	4.25	-1.17E-03	-1.21E-03	-7.21E-04	3.93E-04	3.93E-04	8.73E-04	8.86E-04	9.40E-04	9.83E-04	-6.51E-05
8.00	4.96	-1.17E-03	-1.18E-03	-6.96E-04	3.76E-04	3.76E-04	8.27E-04	8.24E-04	8.47E-04	8.72E-04	-1.21E-04
9.00	5.67	-1.05E-03	-1.06E-03	-6.25E-04	3.37E-04	3.37E-04	7.43E-04	7.40E-04	7.61E-04	7.83E-04	-1.09E-04
10.00	6.38	-8.50E-04	-9.26E-04	-5.93E-04	3.13E-04	3.13E-04	7.32E-04	7.92E-04	9.23E-04	1.01E-03	1.12E-04
11.00	7.08	-7.64E-04	-8.21E-04	-5.00E-04	3.33E-04	3.33E-04	7.11E-04	7.54E-04	8.53E-04	9.20E-04	1.06E-04
12.00	7.79	-6.55E-04	-7.04E-04	-4.29E-04	2.86E-04	2.86E-04	6.10E-04	6.47E-04	7.32E-04	7.90E-04	9.12E-05
13.00	8.50	-5.97E-04	-6.70E-04	-4.23E-04	2.95E-04	2.95E-04	6.34E-04	6.94E-04	8.21E-04	9.03E-04	1.80E-04
14.00	9.21	-4.85E-04	-5.45E-04	-3.45E-04	2.39E-04	2.39E-04	5.15E-04	5.64E-04	6.68E-04	7.35E-04	1.48E-04
15.00	9.92	-3.75E-04	-4.22E-04	-2.67E-04	1.84E-04	1.84E-04	3.98E-04	4.37E-04	5.18E-04	5.70E-04	1.15E-04
16.00	10.63	-2.68E-04	-3.02E-04	-1.92E-04	1.32E-04	1.32E-04	2.85E-04	3.13E-04	3.71E-04	4.09E-04	8.32E-05
17.00	11.33	-4.77E-04	-4.73E-04	-2.25E-04	2.92E-04	2.92E-04	5.04E-04	4.93E-04	4.85E-04	4.86E-04	1.60E-05
18.00	12.04	-5.53E-04	-6.16E-04	-4.32E-04	1.22E-04	1.22E-04	3.88E-04	4.40E-04	5.49E-04	6.18E-04	5.49E-05
19.00	12.75	-1.53E-04	-1.71E-04	-1.20E-04	3.37E-05	3.37E-05	1.08E-04	1.22E-04	1.53E-04	1.72E-04	1.55E-05
20.00	13.46	0.00E+00	0.00E+00	0.00E+00	0.00E+00	0.00E+00	0.00E+00	0.00E+00	0.00E+00	0.00E+00	0.00E+00

Tabella 10.5: microepsilon

The formula above, after a few passages, can be expressed as:

$$1^e * \eta^c = \int \left(\frac{M_z^{*c} M_z^e}{EJ_z} - \frac{M_x^{*c} M_x^e}{EJ_x} \right) dy \tag{10.36}$$

where:

$$M_x^{*c} = -\frac{M_x^c + M_z^c j_z}{1 - j_x j_z} \tag{10.37}$$

$$M_z^{*c} = \frac{M_z^c + M_x^c j_x}{1 - j_x j_z} \tag{10.38}$$

with M_x^c and M_z^c we have indicated the moments of real congruent system and with M_x^e ed M_z^e the moments of the balanced system, that is, due to the application of the load unit explorer.
Then we have to evaluate separately the deflection in the x direction and the deflection in the direction z. For deflection along x, you go to put a unit explorer load in the x direction, whereas the deflection along z arises a unified explorer load in the z direction, section by section. These operations have provided the results reported in figure 10.5.

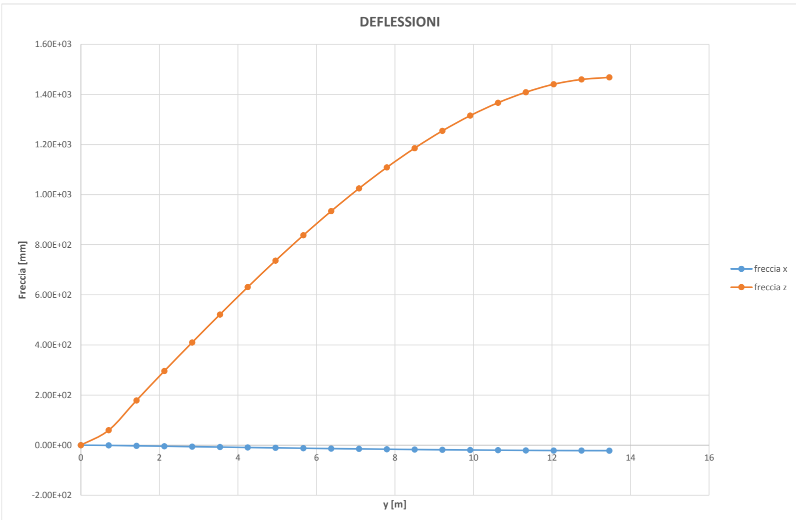

Figura 10.5: Wing deformation over wingspan

Obviously the deflection along x is clearly inferior to that vertical: to tip it has a displacement of about 21.8 mm in the x direction and about 1.47 m in the z direction.

Capitolo 11

“Victoria Huracan - XVIII”

Figura 11.1: “Victoria Huracan-XVIII”

Bibliografia

[1] Prof. Ing. G. Romeo, Ing. Enrico Cestino *Appunti del Corso di Progettazione di Veicoli Aerospaziali*

[2] ATR *Turboprop Market Forecast*

[3] Bombardier *Bombardier Market Forecast*

[4] Embraer *Embraer Market Forecast*

[5] Boeing *Boeing Market Forecast*

[6] Airbus *Airbus Market Forecast*

[7] ICD Research Analysis *The Global Military Aircraft Market 2011-2021*

[8] ATR FAMILY *ATR DC/E. 1, allée Pierre Nadot, 31712 Blagnac cedex, France*, 2014.

[9] D. P. Raymer, *Aircraft Design: A conceptual approach AIAA Education Series*

[10] *Long Range Aircraft - AEA Requirements*, December 1987

[11] European Aviation Safety Agency *EASA Type-Certificate Data Sheet (EASA.(IM).E.049) Pratt&Whitney Canada PW150 Series*, 19 November 2014.

[12] E. Torenbeek *Synthesis of Subsonic Airplane Design* - Delft University Press, 1976.

[13] L.R. Jenkinson, P. Simpkin, D. Rhodens *Civil Jet Aircraft Design* - American Institute of Aeronautics and Astronautics, 1999.

[14] L.R. Jenkinson and J.F. Marchman *Aircraft design projects for engineering student* - American Institute of Aeronautics and Astronautics, 2013.

[15] Smithsonian *National air and space museum*

[16] M.I. Skolnik *Introduction to Radar Systems* - McGraw Hill

[17] M.I. Skolnik *Radar Handbook* - McGraw Hill

[18] M.R. Bell, R.A. Grubbs *JEM modelling and measurements for radar target identification* - IEEE Trans. On Aerospace and Electronic Systems, January 1993

[19] J. Martin, M. Mulgrew *Analysis of the theoretical radar return signal from aircraft propeller blades* - Proceedings of the IEEE Int. Radar Conf. 1990

[20] Air Force Technology *C-295 M Twin-Turboprop Transport Aircraft*